DYNAMIC ANALYSIS OF CONFINED GEOMATERIAL SUBJECTED TO VIBRATORY LOADING

A DISSERTATION

SUBMITTED IN PARTIAL FULFILLMENT OF THE REQUIREMENTS FOR THE
AWARD OF THE DEGREE
OF

MASTER OF TECHNOLOGY
IN
GEOTECHNICAL ENGINEERING

Submitted by:

Ammu Boban

(2K21/GTE/05)

Under the supervision of

Prof. Ashutosh Trivedi

DEPARTMENT OF CIVIL ENGINEERING
DELHI TECHNOLOGICAL UNIVERSITY
(Formerly Delhi College of Engineering)
Bawana Road, Delhi-110042

May 2023

DELHI TECHNOLOGICAL UNIVERSITY
(Formerly Delhi College of Engineering)
Bawana Road, Delhi-110042

CANDIDATE'S DECLARATION

I, Ammu Boban, Roll No. 2K21/GTE/05, student of M. Tech (Geotechnical Engineering), hereby declare that the project dissertation entitled "Dynamic Analysis of Confined Geomaterial Subjected to Vibratory Loading" which is submitted by me to the Department of Civil Engineering, Delhi Technological University, Delhi in partial fulfillment of the requirement for the award of the degree of Master of Technology, is original and not copied from any source without proper citation. This work has not previously formed the basis for the award of any Degree, Diploma Associateship, Fellowship or other similar title or recognition.

Place: Delhi   (AMMU BOBAN)

Date: May 31, 2023

CERTIFICATE

I hereby certify that the Project Dissertation entitled "Dynamic Analysis of Confined Geomaterial Subjected to Vibratory Load" which is submitted by Ammu Boban, Roll No. 2K21/GTE/05, to the Department of Civil Engineering, Delhi Technological University, Delhi in partial fulfilment of the requirement for the award of the degree of Master of Technology, is a record of the project work carried out by her under my supervision. To the best of my knowledge, this work has not been submitted in part or full for any Degree or Diploma to this University or elsewhere.

Place: Delhi

Date: May 31, 2023

(Prof. ASHUTOSH TRIVEDI)

Professor & Supervisor

Department of Civil Engineering

ABSTRACT

The reinforcement using single-layer geogrid on a confined geomaterial is an effective way of solving practical problems. With the use of multi-layered reinforcement, this study aims to offer a superior alternative design for supporting heavy loads on geomaterial. The location of reinforcement plays a crucial role in the overall strength. The experimental investigations were conducted on poorly graded sand (SP) whose angle of internal friction and cohesion are $36.6°$ and 4.4 kPa, respectively. The effect of single-layer geogrid reinforcement placed at different depths of the geomaterial was evaluated. Further, the bearing capacity of the geomaterial was compared for single, double and triple-layered geogrid reinforcement. A laboratory Digital Static Cone Penetration Test (DSCP) was performed to assess the load-displacement behaviour of unreinforced and reinforced geomaterial. The result shows that reinforced geomaterial achieved higher resistance compared to unreinforced systems. An optimum combination of placement depths of double-layered reinforcement is proposed.

Additionally, the dynamic response of the confined geomaterial subjected to vibratory load has been investigated using a numerical program supported by experimental findings. An accelerometer has been used to report the acceleration, velocity, and displacement of confined geomaterial fill along the depth at varied frequencies of vibratory load. Further, the experimental findings were used in the numerical program to obtain the shear modulus and damping of confined geomaterial. The stress-strain response shows compounded effects with an increase in frequency and modulus of elasticity. It has been observed that displacement is amplified by 10-90 % for a frequency range of 5-75

Hz. The shear stress-strain results showed that the shear modulus is magnified by 50 % for varied input parameters considered in the study. The damping of the confined geomaterial has been found to be 0.5-5 % for varied unit weight inputs (16 - 22 kN/m^3). The results are compared with the outputs obtained by numerical simulation and experimental analysis for estimating the dynamic properties of the confined geomaterial subjected to vibratory load.

Further, the study utilized various numerical simulation and experimental data to train and evaluate different models to generate predictions. These predictions were essential for the research. The models employed included ensemble boosted tree, squared exponential Gaussian Process Regression (GPR), Matern 5/2 GPR, exponential GPR, and decision tree architectures (fine and medium). These models greatly facilitated the analysis of the collected data and enabled accurate result predictions. Among the examined models, the Matern 5/2 GPR model exhibited exceptional accuracy with an R^2 value of 0.99, demonstrating its remarkable predictive capability. The outcomes highlight the proficiency of the Matern 5/2 GPR and Boosted Tree models in forecasting displacement patterns and enhancing the comprehension of the relationship between displacement and depth. The outcomes of the present study can effectively be adopted by engineers and partitioners for estimating the dynamic properties of the confined geomaterial in construction practices.

ACKNOWLEDGEMENT

TABLE OF CONTENTS

LIST OF TABLES

LIST OF FIGURES

LIST OF SYMBOLS, ABBREVIATIONS AND NOMENCLATURES

γ	-	unit weight
D_r	-	relative density
P I	-	plasticity index
$\sigma`_c$	-	effective confining pressure
OCR	-	over-consolidation ratio
f	-	frequency of loading cycle
N	-	number of cycles
G	-	shear modulus
D	-	damping ratio
DSCPT-		digital static cone penetration test
q_c	-	cone resistance
AVD	-	acceleration velocity displacement
C_u	-	coefficient of uniformity
C_c	-	coefficient of curvature
MDD	-	maximum dry density
OMC	-	optimum moisture content
C	-	cohesion
ϕ	-	angle of internal friction
LVDT	-	linear variable displacement transducer
μ	-	Poison's ratio
E	-	Young's modulus
ψ	-	dilation angle
ρ	-	density
FEA	-	finite element analysis
τ	-	shear stress
x	-	displacement
z	-	depth
GPR	-	gaussian process regression
CRRF	-	classification and regression random forests

ANN   -   artificial neural networks

ANFIS -   adaptive network-based fuzzy inference system

MRM   -   multiple regression analysis method

MLP   -   multi-layer perceptrons

ANN-DFO-   artificial neural network-dragonfly optimizer

RF   -   random forest

SPS   -   soil-pile-structure

ML   -   machine learning

MSE   -   mean squared error

RMSE -   root mean squared error

MAE   -   mean absolute error

DT   -   decision tree

R^2 -   coefficient of determination

CHAPTER 1
INTRODUCTION

The following chapter will help understand the response of confined geomaterial, which is stabilized by reinforcing with the geosynthetic material. A numerical program has been adopted to analyze the behavior of confined geomaterial.

1.1 GENERAL INTRODUCTION

The vibrations developed by dynamic load of earthquakes, machine foundations, wind, and pavements are very crucial while determining the strength of the geomaterials supporting these structures (Bourdeau et al., 2002). The shear stiffness (G) and dissipation of energy by calculating damping ratio (D) are the key dynamic parameters in the sand at low strain levels. The equation to determine the damping ratio is given by,

$$D = \frac{W_D}{4\pi W_s} \tag{1}$$

W_D is the energy dissipated and W_S is the strain energy. The shear stress-strain hysteresis loop can also be used to compute the damping ratio by calculating the area under it. Soil research is conducted on geomaterial to estimate its dynamic properties. Dynamically loaded soil experiences cyclic stresses with varying amplitudes and frequencies.

Various kinds of research are focused on sand to propose relationships of shear stiffness, damping ratio, and stiffness (Iwasaki and Tatsuoka, 1978, Seed et al., 1986, Ishibashi and Zhang, 1993, Rollins et al., 1998, Gupta and Trivedi, 2009, and Ojha and Trivedi, 2013). The shaking table test is the most common among them (Brennan et al., 2005, Yang et al., 2011, Yoo et al., 2013, Conti et al., 2014, Maze, 2017, Price et al., 2017, Fathi et al., 2020, Reddy and Krishna, 2021, and Alshawmar and Fall , 2022). The dynamic properties are significantly influenced by a number of variables, including number of cycles (N), type of soil, composition of the soil, frequency of loading cycle (f), over-consolidation ratio (OCR), relative density (D_r), effective confining pressure (σ'_c), plasticity index, and shear strain amplitude (γ). It has been demonstrated that the void ratio, shear strain amplitude, and effective stress level have the most effects on shear modulus in clean

sands. (Wichtmann and Triantafyllidis, 2004, Zhang et al., 2005, and Zeghal et al., 1995) These were also thought to have an impact on damping to have an impact on damping as well, with the number of loading cycles serving as another important consideration. For clays, the number of loading cycles has been linked to a drop in shear modulus and an increase in pore pressure. In addition, the over-consolidation ratio and plasticity index have an effect on how clay behaves. The main input variables for dynamic evaluations in numerical soil models are shear stiffness and damping with strain level fluctuations, sometimes referred to as shear stiffness - shear strain amplitude and damping ratio - shear strain amplitude curves. It is critical to comprehend how soils behave under cyclic shear stress-shear strain in order to forecast how sites will respond to applied shear loads.

Determining the dynamic properties of pure sand is the major objective of the study. Stress analysis and displacement are the two main components of the dynamic analysis technique. These are carried out using the finite element programme Abaqus 2017, and the findings are validated using an experimental setup. An accelerometer was used to determine acceleration, velocity, and displacement, over a range of distances. Accelerometers are electromechanical sensors that produce electrical charges proportional to the force exerted upon them.

1.2 CONE PENETRATION TEST

Cone penetration testing is critical in geotechnical engineering, particularly in the building of pavements and other civil constructions. Cone Penetration Tests (CPT) are required for transportation (Kumar et al., 2020) related projects, including subsurface investigation for new structure building and restoration work. The widely used techniques for soil exploration include in-situ, dynamic cone penetration tests (DCPT), standard penetration tests (SPT), and plate load tests (Kumari and Trivedi, 2022).

The CPT can be used in dry, saturated or wet sand (Kluger et al., 2021, Bonita, 2020, Miller et al., 2018, Pournaghiazar et al., 2013, Shaqour et al. 2007, Baldi et al., 1982, and Almeida et al., 1991). A comparison study on the suction profiles, tip resistance and skin friction tells us how CPT parameters are influenced by moisture content and soil suction (Collins and Miller, 2020). CPT measurements can be beneficial to determine initial horizontal stress and relative density (Ahmadi and Dariani, 2017). CPT done on carbonate

fill which was undertaken in the centrifuge showed that the empirical relationship set for silica sand should not be used for carbonate sands (Giretti et al., 2018).

The usage of geogrid under static or cyclic load to improve settlement behaviour has gained significant attention. In the road building sector, the usage of geosynthetics, or as it was known then, "geotechnical fabrics," was growing in popularity by 1980. Roadway subgrades with poor or weak soil are routinely improved using geosynthetic layers as reinforcement (Cuelho and Perkins 2017, Sigurdsson, 1993, Singh et al., 2022). This study aims to determine the influence while placing geomaterial at various intervals within the subgrade using the Digital Static Cone Penetration Lab Test. Pure-cleaned Yamuna sand is tested as the soft subgrade, in which single, double and triple-layered geogrid reinforcement is used to enhance the strength. The study finds out the optimum depth at which we have to place the geogrid and the optimum number of layers.

1.3 MACHINE LEARNING TECHNIQUES

Machine learning is a powerful and rapidly evolving field of artificial intelligence that focuses on developing algorithms and models that enable computers to learn and make predictions or decisions without explicit programming. It revolves around the idea of training computers to recognize patterns and extract meaningful insights from large and complex datasets. By employing statistical techniques, ML algorithms iteratively learn from data, improving their performance over time. This technology has revolutionized various industries, including finance, healthcare, marketing, and more, by enabling advanced data analysis, automation, and prediction capabilities. With its ability to handle massive amounts of information and adapt to changing conditions, machine learning holds immense potential for solving complex problems and driving innovation across numerous domains.

Predicting soil displacement caused by vibratory stress using machine learning (ML) poses several challenges. One major issue is the scarcity of high-quality datasets that encompass a wide range of soil qualities, input parameters, and corresponding displacement measurements under vibratory loading conditions. Acquiring such datasets is crucial for effectively training and validating ML models. Moreover, the understanding and interpretation of ML models in the field of geotechnical engineering remain complex. The development of interpretable ML models would significantly enhance the acceptance

and utilization of ML techniques within the geotechnical engineering community, providing valuable insights into the underlying behaviour of soil.

In this study, the data collected from numerical and experimental simulations underwent a series of processing steps. Models were carefully selected to capture the underlying patterns in the data, and then they were trained and evaluated using appropriate techniques. The predictions generated by these models were of particular interest in this study. The models employed included fine and medium decision tree structures, as well as the Matern 5/2 Gaussian Process Regression (GPR), Rational Quadratic GPR, Squared Exponential GPR, Exponential GPR, and Boosted Tree models. These models were chosen based on their suitability for the specific task at hand and their potential to provide accurate predictions.

1.4 ORGANISATION OF CHAPTERS

This project report includes the following chapters:

The project title has been thoroughly introduced in Chapter 1. The major objectives and general framework of the work have been described.

The analysis of the research articles and their findings are discussed in Chapter 2. There have been established and noted study gaps after reading several research articles and books.

The materials utilised in this project and the methods employed have both been explained in Chapter 3.

The findings of this study have been listed and extensively discussed in Chapter 4.

The conclusions from the research are outlined in Chapter 5 along with suggestions for future investigation.

CHAPTER 2
LITERATURE REVIEW

2.1 INTRODUCTION

Numerous dynamic stresses, including as traffic or seismic loads, machine foundations, and piling, may be applied to clay or sandy soils (Koga and Matsuo, 1990, Okur and Ansal, 2007, Vucetic and Mortezaic, 2015). Depending on their purposes, dynamic loads in soil dynamics can be applied at different frequencies. In this regard, damping ratio, denoted by D, and shear modulus, indicated by G, are two of the dynamic parameters used in geotechnical analysis and design the most often. Different testing techniques, such as the piezoelectric bender element test, the cyclic simple shear test, the resonant column test, and the cyclic triaxial test, have been used by many studies to determine the dynamic characteristics of different soils at different strain levels.

2.2 REVIEWS OF LITERATURE

- Kluger et al. (2021) found that there was little variation in cone resistance between samples that were soaked and those that were dry. Dry samples typically displayed somewhat greater consolidation stresses than saturated samples at the lower cone resistance, but at the higher consolidation stress, there was no obvious difference between the dry and saturated conditions.

- Molina-Gómez et al. (2020) focused on the small-strain response and investigated the effects of mean effective stress on the soil stiffness and void ratio. The Resonant Column findings demonstrated that, for sand strain levels range greater than 10^5, the damping ratio rises. Results also indicated that when $\sigma`_c$ grows, D declines.

- According to Singh et al. (2020), the depth and profile of the test section allowed DCPT to detect important variations in the strength and stiffness of the base and subgrade layers. It can also be used to indicate where the base layer and subgrade layer meet. However, because the device was unable to penetrate up to the depth of the reinforcing layer with the application of stress, the DSCPT data did not reveal changes in the layer.

- According to Miller et al. (2018), compared to non-plastic soils, soils with significant plasticity have a greater dependency on suction for tip resistance. Given that the range of matric suction is much wider and, hence, has a far greater influence on the shear strength of clayey soils, this is to be anticipated.

- To assess the dynamic characteristics across a broad range of shear strain, saturated Brahmaputra sand was subjected to strain-controlled cyclic triaxial testing by Kumar et al. (2020). Hysteresis loops during various loading cycles showed the dynamic behaviour of the soil and had a pronounced asymmetry, especially at higher strain levels. Variations in $\sigma`_c$ and D_r are seen to have a considerable impact on the shear modulus (G) of soil.

- According to Ahmadi and Dariani (2017), physical model tests of the CPT (calibration chamber) in sand have sufficiently demonstrated that the cone tip resistance is mostly influenced by in-situ horizontal tension and relative density.

- Amir-Fayer et al. (2017) employed a number of model forms to forecast the dynamic behaviours of soils, concentrating especially on the shear modulus and material damping, given that the majority of the models currently in use were constructed experimentally for specific soil types, strain ranges, etc. A process of model selection and application was carried out on soils, polypropylene fibrillated fibre, and clay composites in order to best match empirical data. A shear modulus form and a typical damping model form were developed to connect the dynamic properties of soil materials to shear strain. The proposed functions could replicate shear modulus and damping behaviour within the strain amplitude range of typical earthquakes. According on the results of the mathematical modelling, the suggested model functions may be used to simulate a range of soil types and fiber-soil composites.

- Gomes et al. (2016) discovered that in sands, the damping factor may be effectively reduced, and the stiffness and damping curves for hysteretic loops and strain-dependent systems exhibit good agreement. Although it also significantly affects the soil stiffness, clays also achieve the reduction in damping for big stresses. Due to the maximum shear strain level reached in sands, numerical simulations revealed that the new parameter has no discernible impact on the seismic soil response, whereas clays experience a drop in both damping and stiffness.

6

- In their study, Wichtmann and Triantafyllidis (2013) examined the impact of grain size distribution on G and D at various strain levels, including the extremely tiny to medium strain range. It was shown that the G/G_{max} and damping ratio are related to the uniformity coefficient (C_u), with a rise in C_u causing a significant decline in the modulus ratio and a rise in the damping ratio.

- In a database of different sands created by Oztoprak and Bolton (2013), the shear modulus degradation curves from 454 experiments that were mentioned in the literature were included. They suggested a hyperbolic equation as the best-fit functional relationship for the deterioration of the shear modulus of granular soils based on this data.

- According to Trivedi and Singh (2004), the relationship between shear strength and penetration resistance is established using data on relative density, peak friction angle, and mean confining pressure in relation to the relative dilatancy of the ash. For the relative density of the ash fill and the depth of cone penetration, they suggested altering the bearing capacity factor.

- Darendeli (2001), Hardin and Black (1968), and Vucetic and Dobry (1991) have studied the dynamic behaviour in both over and normal -consolidated clays. They found that the plasticity index (PI) had a substantial effect on each strain amplitude and came to the conclusion that as PI increases, while the damping ratio falls, the ratio of the shear modulus to the maximum shear modulus increases.

- Assimaki et al. (2000) provided a simple four-parameter model to describe the shear stiffness factors and damping coefficients for a granular soil exposed to horizontal shear pressures brought on by vertically propagating shear waves. The simulations demonstrate that, when confining pressure is taken into account, soil elasticity increases gradually increasing depth. One of the alleged shortcomings of the standard equivalent-linear model, that it unrealistically wipes out the high frequency components of motion when used for moderately deep to very deep soil profiles, is significantly reduced by the refinement brought about by the pressure-dependent characterization of the soil.

- Hardin and Drnevich (1972) found that with increasing strain amplitude, the shear modulus declines and the damping ratio drastically rises based on extensive experiments on a range of disturbed and undisturbed soils. Clean sands are not influenced the same way as cohesive soils. Additionally, they included formulas

and diagrams for estimating the soil shear modulus and damping, which may be used to design issues requiring repetitive loading or soil vibration.

- A recent study by Baghbani et al. (2023) utilized machine learning techniques, specifically Classification and Regression Random Forests (CRRF) and Artificial Neural Networks (ANN), to predict the secant shear modulus and damping ratio of sand. The models demonstrated high accuracy, with correlation coefficients (R^2) of 0.998 and 0.995 for ANN and CRRF, respectively. The study highlighted the significance of relative density, vertical stress, and cyclic stress ratio as influential factors in forecasting the damping ratio and secant shear modulus. Compared to other models in the literature, the ANN and CRRF models outperformed in terms of forecasting and assessing the dynamic characteristics of sand and the impact of input factors. These findings underscore the potential of machine learning in accurately predicting and understanding the behaviour of sand.

- Akbulut et al. (2004) conducted a study comparing the performance of different training methods for parameter estimation in the Adaptive Network-based Fuzzy Inference System (ANFIS) model. The results indicated that the improved hybrid training method used in ANFIS outperformed traditional back-propagation techniques such as Multiple Regression Analysis Method (MRM) and Multi-layer Perceptrons (MLP). The ANFIS model was trained to forecast the shear modulus and damping coefficient of sand samples as an alternative to laboratory testing. When compared to MLP and MRM, the ANFIS model exhibited superior performance in modeling complex soil parameters, demonstrating its efficacy in accurate parameter estimation.

- Hasthi et al. (2022) proposed a novel hybrid approach called ANN-DFO (Artificial Neural Network-Dragonfly Optimizer) to evaluate the displacement amplitude of footings on geocell-reinforced beds subjected to vibration loading. The model was trained and tested using extensive field vibration test data, ensuring its reliability. Compared to other machine learning models like Random Forest (RF), Gaussian Process Regression (GPR), and M-5 rules, the ANN-DFO model exhibited superior performance in forecasting displacement amplitude. Additionally, a sensitivity analysis was conducted to identify the key input factors that significantly influenced the estimation.

- Sharma et al. (2019) employed genetic programming and Artificial Neural Network (ANN) techniques to develop predictive formulas for estimating displacement amplitude, taking into account multiple input factors. The genetic programming model exhibited superior performance compared to the ANN model in predicting the system's reaction. Both models showed strong agreement with the results obtained from field tests. The analysis revealed that the operating frequency had the most significant impact on displacement amplitude.

- Farfani et al. (2015) conducted a study on the seismic analysis of soil-pile-structure (SPS) systems, employing data-based approaches to develop a mathematical model. They compared the performance of their neural network model with the finite element technique and found that the neural network model, with two hidden layers, effectively predicted the dynamic properties and seismic response of the SPS system. The study highlights the importance of generating more experimental data and utilizing data-based techniques to overcome the limitations of traditional analytical methods in addressing complex dynamic analysis problems in SPS systems.

2.3 RESEARCH GAP

The following study gaps were revealed by reading through several research articles, books, and codal provisions.

- There are limited number of researches on digital static cone penetration test for the optimum number of layers and the optimum combination of double-layer of geogrid reinforcement in confined geomaterial.

- There is a lack of agreement about the validity and accuracy of displacements derived from accelerations. The accurate estimates of permanent displacements from recorded accelerograms are required.

- There is a lack of statistical comparison and verification between the expected findings and experimental data to find out the dynamic property of confined geomaterial when subjected to vibratory loading.

- While ML applications in geotechnical engineering have been extensively explored for various geotechnical problems, such as slope stability and settlement prediction, there has been limited research specifically dedicated to predicting soil displacement under vibratory stresses using ML techniques.

2.4 OBJECTIVES OF THE STUDY

- To find out the optimum number of layers of geogrid reinforcement in confined geomaterial using cone penetration test.
- To figure out the optimum combination of double-layered geogrid reinforcement in confined geomaterial using a digital static cone penetration test.
- To conduct Acceleration, Velocity, and Displacement (AVD) analysis of the confined geomaterial using a dynamic shaking unit.
- To compare the numerical and experimental findings.
- To determine the dynamic properties of confined geomaterial.
- To process the collected values and select, train, and evaluate models for making predictions.
- To assess the performance of different models, including fine and medium decision tree structures, matern 5/2 GPR, rational quadratic GPR, squared exponential GPR, exponential GPR, and boosted tree, in predicting soil displacement.
- To investigate the suitability of ML models for predicting soil displacement under vibratory stresses.

CHAPTER 3
MATERIALS AND METHODS

The most common rivers in India are the Ganga, Yamuna, Brahmaputra, Godavari, Kaveri, and Indus. Sand is most commonly found on the banks of the river. The Yamuna River provided the geomaterial that was employed for this investigation. To get rid of any impurities, it was carefully cleansed. Sieve analysis was conducted on the geomaterial to find out the gradation. In addition to this test, the Direct shear test, standard proctor test and Pycnometer tests were conducted. The sections that follow will provide a description of the tests.

3.1 PREPARATION OF THE SAMPLE

The geomaterial collected was found to have impurities, hence it was cleaned thoroughly. The cleaning was done through a 75 μm IS sieve. Any particles below 75 μm were removed through washing. The clean sample was air-dried for 24 – 48 hours according to the weather condition. Hence clean and dry sand was used for the experiment. Fig. 1 shows the cleaned sample before and after drying.

<div align="center">(a)   (b)</div>

Fig. 1. Sand used for experiments (a) before and (b) after air-drying

3.2 SIEVE ANALYSIS

As per IS:2720 (Part 4) – 1985 sieve analysis was conducted before and after the cleaning. A portion of geomaterial was taken to pass through 4.75, 2, 1.18, 0.6, 0.3, 0.15, and 0.075-

mm sieve as shown in Fig. 2. The mass of geomaterial retained on each sieve was weighed to calculate the percentage finer. Table 1 shows sieve sizes and percentage finer for before and after cleaning. Fig. 3 shows the gradation curve before and after cleaning.
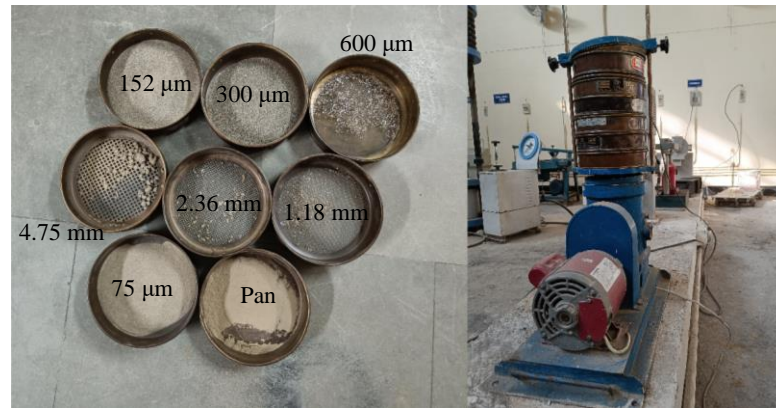
Fig. 2. Grain-size distribution by sieve analysis

Table 1. Table showing sieve sizes and percentage finer for before and after cleaning

Sieve sizes (mm)	% Finer (Before cleaning)	%Finer (After cleaning)
4.75	99.9	99.6
2	99.7	99.2
1.18	99.2	98.8
0.6	98.6	98
0.3	49.7	53.6
0.15	13.6	11.2
0.075	4	0
Pan	0	0

The curve in fig. 3(a) gives the values of D_{10}, D_{30}, and D_{60} before cleaning which are 0.123, 0.215, and 0.352 respectively. The computed values for uniformity (C_u) and curvature (C_c) coefficients are 2.86 and 1.07 respectively. The curve in Fig. 3(b) was used to compute the values of D_{10}, D_{30}, and D_{60} after cleaning; the results were 0.145, 0.214, and 0.335, respectively. Estimates for the uniformity (C_u) and curvature (C_c) coefficients were also provided, and they were 2.31 and 0.94, respectively. As a result, the geomaterial is categorised as poorly graded sand (SP) according to IS:2720 (Part 4) – 1985.
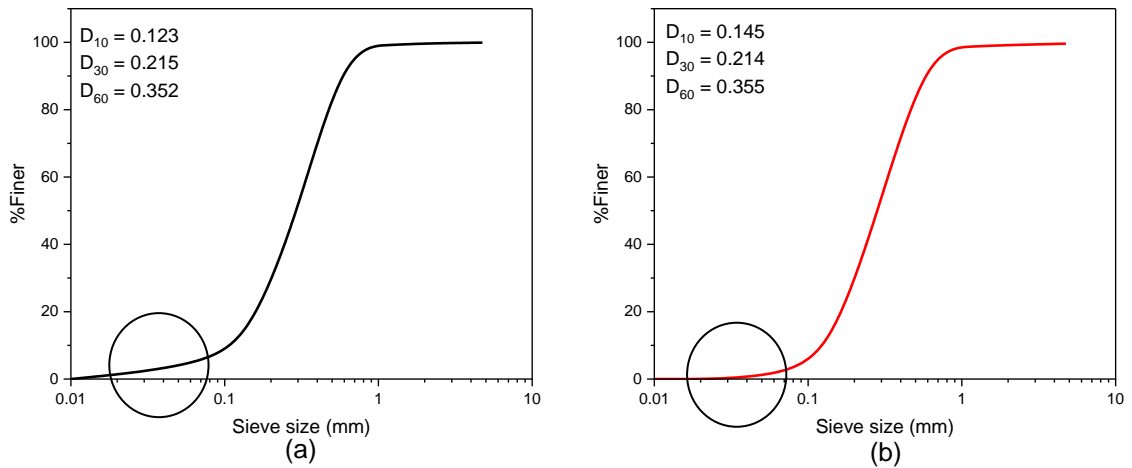
Fig. 3. Grain-size distribution curve (a) before and (b) after cleaning. The circled portion in in (b) indicates the removal of fines

3.3 SPECIFIC GRAVITY TEST

Calculating soil parameters like void ratio and saturation level requires an understanding of specific gravity. This dimensionless unit is the ratio of material density to the density of water. A specific gravity test was conducted confirming to IS:2720 (Part 3) – 1980. Pycnometer is used for the test is shown in Fig. 4. The pycnometer is a 1 litre glass jar with a brass conical lid attached to the top. At the top, there is a 6 mm-diameter hole. By placing a washer between the cap and the jar, the leak is stopped. To ensure that the volume of the pycnometer remains constant during the computation, the jar is screwed shut all the way. To the nearest 0.001 g, the entire pycnometer with a conical top is weighed. Weigh the bottle, 50 g of oven-dried sample, conical top, and other components to the closest 0.001 g. To ensure that the soil in the bottle is barely covered, enough air-free distilled water must be added. The bottle containing the sample and water must be put into the vacuum desiccator, which must then gradually expel the air.

Fig. 4. Specific gravity determination by Pycnometer

With the spatula, carefully swirl the sample in the bottle. The bottle and its contents must then be taken out of the desiccator and filled with more air-free distilled water. After that, the conical top should be put in. Drying off the pycnometer, the entire apparatus is then weighed to the closest 0.001 g. The container must next be thoroughly cleaned, entirely filled with distilled water without any air pockets, dried, and weighed to the closest 0.001 g.

$$\text{Specific Gravity} = \frac{m_2 - m_1}{(m_4 - m_1) - (m_3 - m_2)} \qquad (2)$$

where,

m_1 = Weight of the bottle (g)

m_2 = Weight of bottle and the soil sample (g)

m_3 = Weight of bottle, soil sample, and water (g)

m_4 = Weight of bottle and water (g)

The value of specific gravity is obtained using the equation (2) is:

Specific gravity = 2.74 before cleaning

Specific gravity = 2.68 after cleaning

3.4 STANDARD PROCTOR TEST

Compaction makes soil more compact by removing air gaps, which densifies the soil. The dry density of a particular soil may be used to determine how compacted it is. The dry density is maximum when the water content is ideal. A 5 kg oven-dried geomaterial was collected in accordance with IS:2720 (Part 7) - 1980. The geomaterial was thoroughly mixed after the appropriate amount of water was introduced. As illustrated in Fig. 5, 25 blows with a 2.6 kg hammer dropped freely from a height of 310 mm above the ground compacted three layers of the moist material into the mould. The compressed geomaterial's weight inside the mould is calculated.
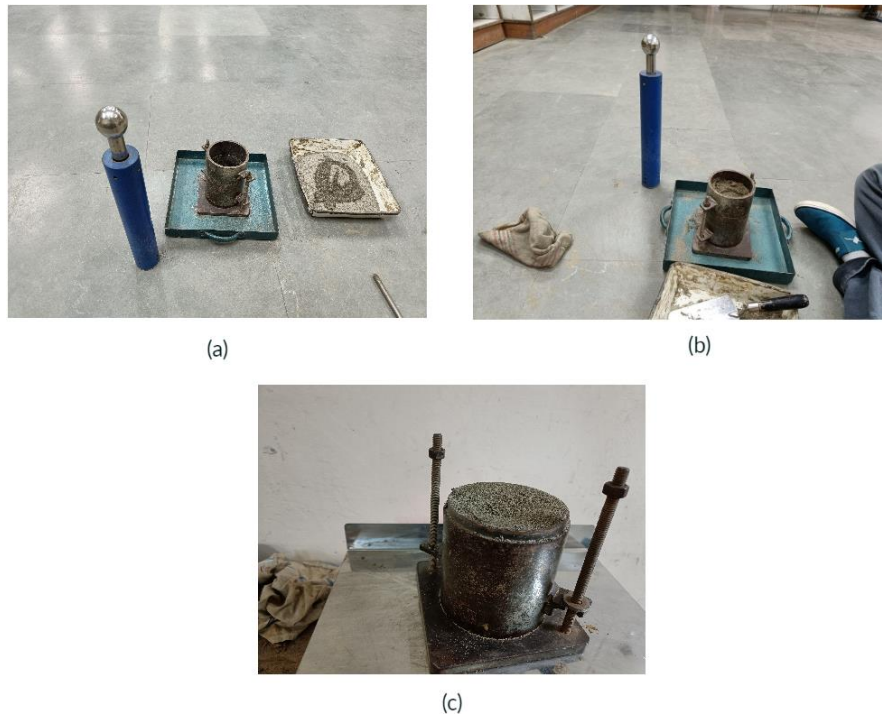
Fig. 5. Figures showing soil sample (a) before compaction (b) while compacting (c) after compaction using standard proctor test

Table 2 provides the determined dry density and moisture content before and after the sand was cleaned. To find the optimum moisture content (OMC) and maximum dry density (MDD), which are found in Fig. 6(a) to be 4.9 % and 16.56 kN/m^3 respectively for sand before cleaning. The MDD and OMC from Fig. 6(b) are 10.4 % and 17 kN/m^3 respectively for sand after cleaning. These are the values when the experiment was repeated with various moisture values.

Table 2. Table showing moisture content and dry density obtained from standard proctor test

Moisture content (%) (before cleaning)	Dry density (kN/m^3) (before cleaning)	Moisture content (%) (after cleaning)	Dry density (kN/m^3) (after cleaning)
2.29	16.19238	3.2	16.127
3.27	16.194	5.5	16.385
4.7	16.5598	7.8	16.7852
6.92	16.423	9.9	16.986
8.92	16.324	11.7	16.921
		13.9	16.654
		15.5	16.459

15
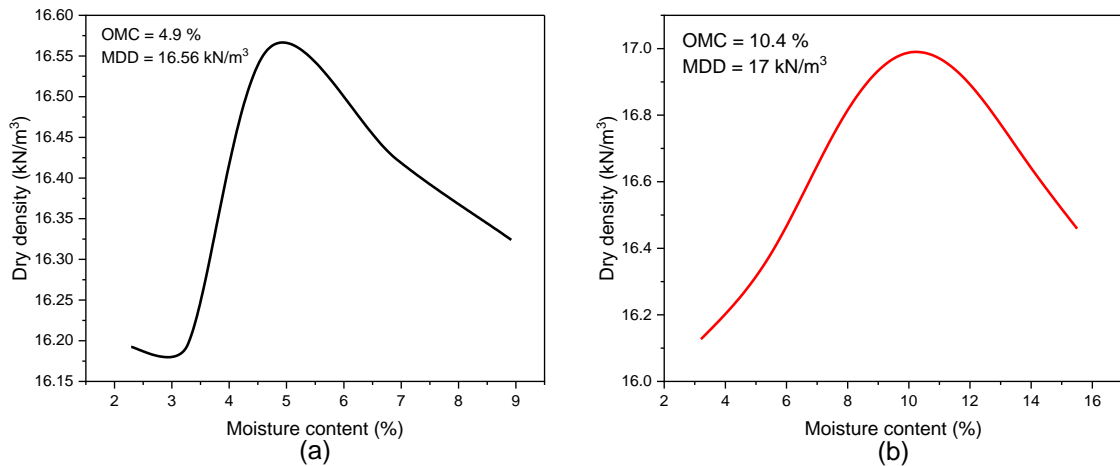
Fig. 6. Standard proctor compaction curve (a) before cleaning and (b) after cleaning

3.5 DIRECT SHEAR TEST

For the direct shear test, the IS:2720 (Part 13) - 1986 standard was adhered to. The geomaterial is tamped into the shear box, which has a porous stone at the bottom and a base plate, grid plate, and other supporting plates. Grid plates are affixed to the top, and it is then placed into place on the loading frame. A standard loading of 0.5 kg/cm^2 is applied from the top, normal of the specimen. Shear was applied horizontally until failure or when longitudinal displacement reached 20 % during the test. The computer automatically logs the data of shear force and horizontal displacement in order to calculate the cohesiveness and angle of internal friction of the geomaterial. It was conducted again with a typical loading of 1 and 1.5 kg/cm^2. Table 3 is a list of the findings before and after the sand was cleaned. The cohesion and angle of internal friction are shown in Fig. 8(a) as 9.47 kPa and 34.27º, respectively before the sand was cleaned. The cohesion and angle of internal friction are shown in Fig. 8(b) as 4.4 kPa and 36.6º, respectively after the sand was cleaned. The digital direct shear test device is depicted in Fig. 7.

16

Fig. 7. Direct shear test apparatus

Table 3 Table showing the values of normal stress and Shear stress from direct shear test

Normal stress (kPa)	Shear stress (kPa) (Before cleaning)	Shear stress (kPa) (After cleaning)
50	38.307	41.36
100	70.7849	78.96
150	130.1498	115.6
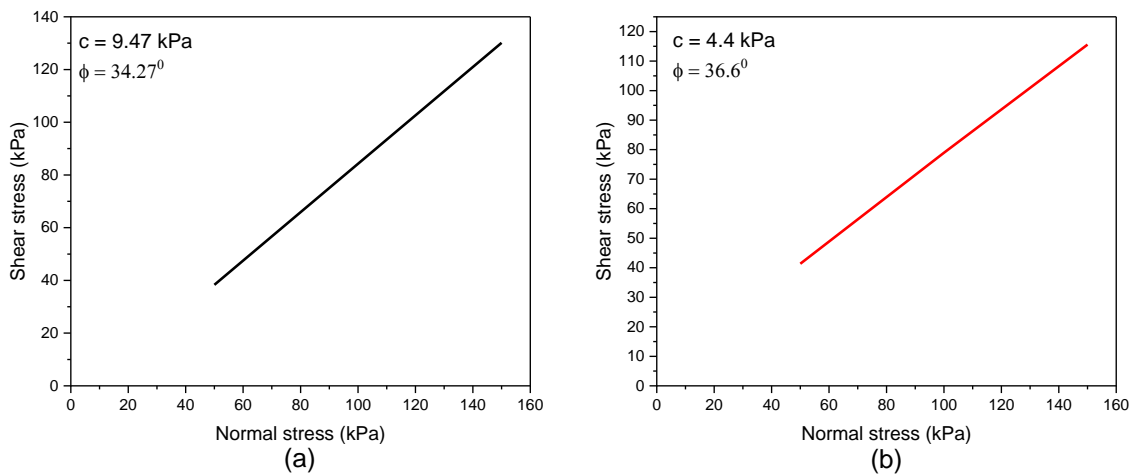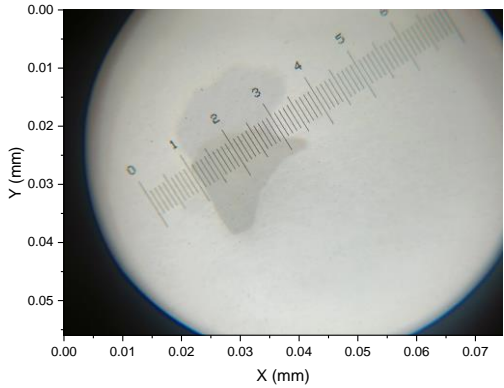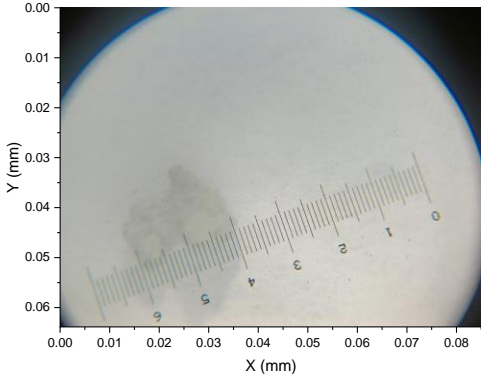
Fig. 8. Normal stress vs shear stress graph from direct shear test

3.6 ANALYSIS OF SAND PARTICLES

Sand is a typical material that has a wide range of uses in several sectors of the economy, including geotechnical engineering, manufacturing, and building. For operations to be optimised and product quality to be maintained, it is essential to understand the properties and makeup of sand particles. By determining the microstructure of sand particles, the

17

Brinell microscope, a tool that combines microscopy with indentation testing, offers a novel method of analysing sand particles. Typically, Brinell microscopes include adjustable magnification capabilities so that the sand particles may be precisely seen. They frequently provide a range of magnification choices to fit different particle sizes and measuring needs. The sand particles of the present paper were studied under a Brinell microscope. Pictures were captured to find out the size and were analysed. The length and angles have been found using OriginPro software. The findings of the analysis have been listed in Table 4. It shows that the sand particles used here are angular. Hence, the Direct shear test shows a high value of cohesion. The angular particles shows interlocking characteristics.

Table 4. Analysis of sand particles for length and angle

Grain No.	Image	Lengths (mm)	Angles
1		0.0142, 0.00572, 0.0218, 0.0155	61.21°, 118.79°, 126.6°, 53.4°
2		0.0187, 0.0099, 0.0167, 0.0187	87.29°, 92.72°, 115.62°, 64.38°
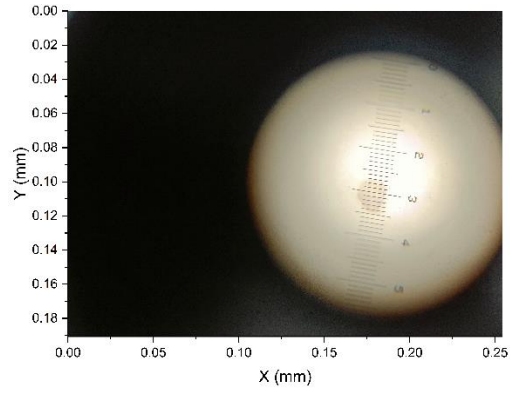
3		0.00678, 0.0127, 0.0134, 0.018	61.35º, 118.65º, 112.19º, 67.83º
4		0.00697, 0.0139, 0.0133	70.43º, 79.98º, 29.59º
5		0.00804, 0.01, 0.0103, 0.00574	47.23º, 132.77º, 70.11º, 109.89º
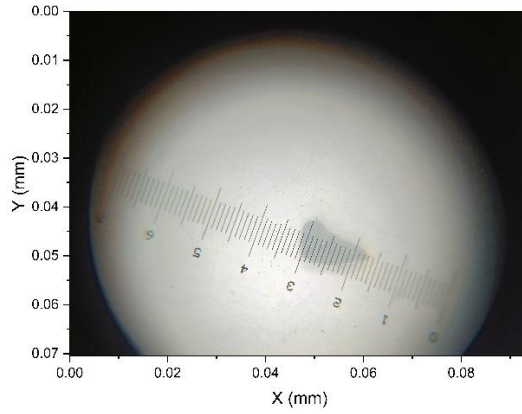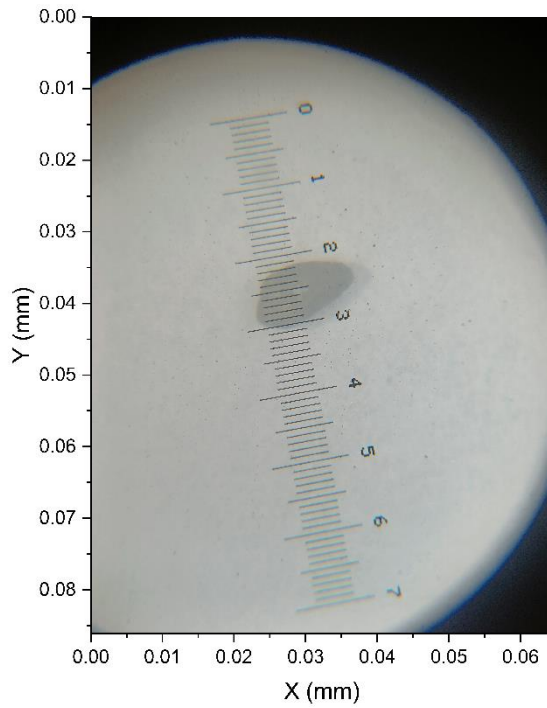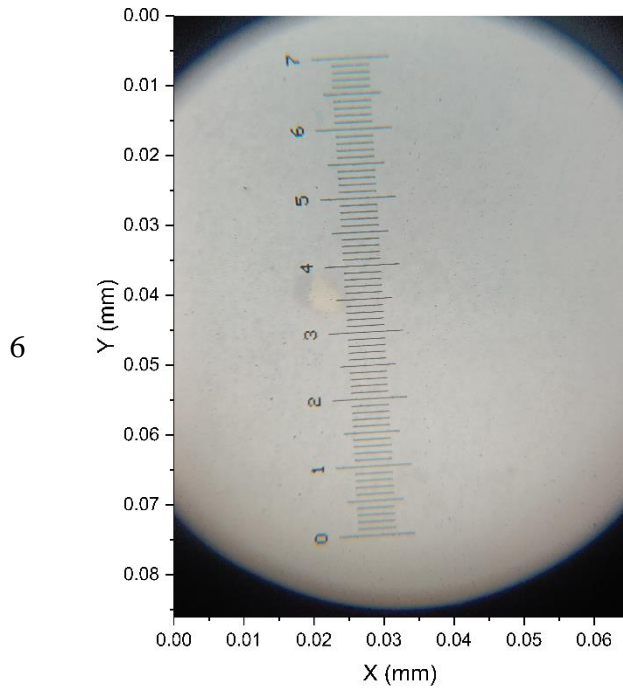
6		0.00432, 0.004, 0.00221, 0.00343	89.14º, 90.86º, 120.97º, 59.03º
7		0.0262, 0.0221, 0.0141, 0.013	66.22º, 113.78º, 83º, 97.01º
8		0.00854, 0.0102, 0.0103, 0.00434	56.77º, 123.23º, 92.49º, 87.52º
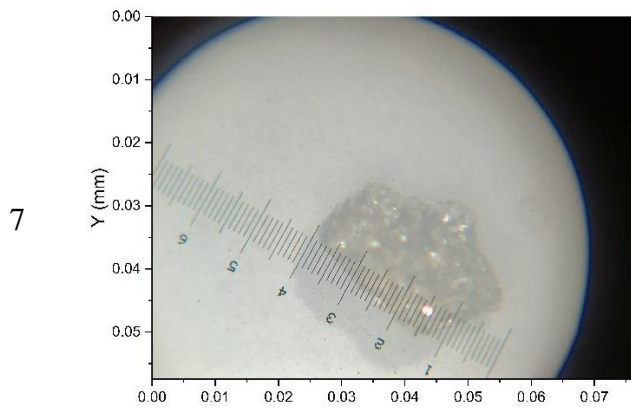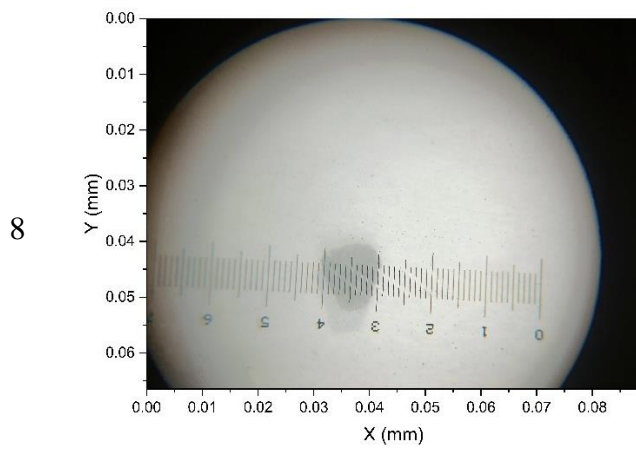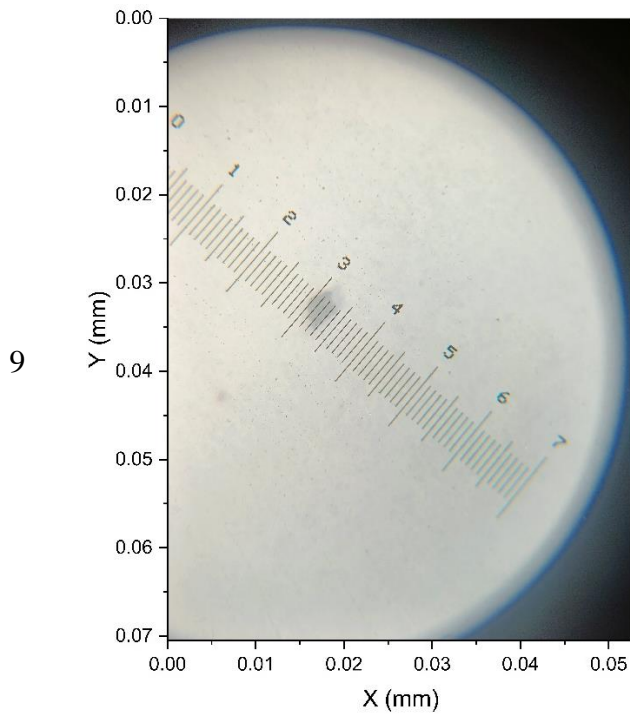
9		0.00296, 0.00351, 0.00362, 0.00211	51.55º, 128.45º, 73.29º, 106.71º
10		0.00221, 0.0045, 0.00275, 0.00329, 0.00397, 0.00437	84.24º, 138.26º, 147.6º, 75.76º, 136.64º, 137.5º
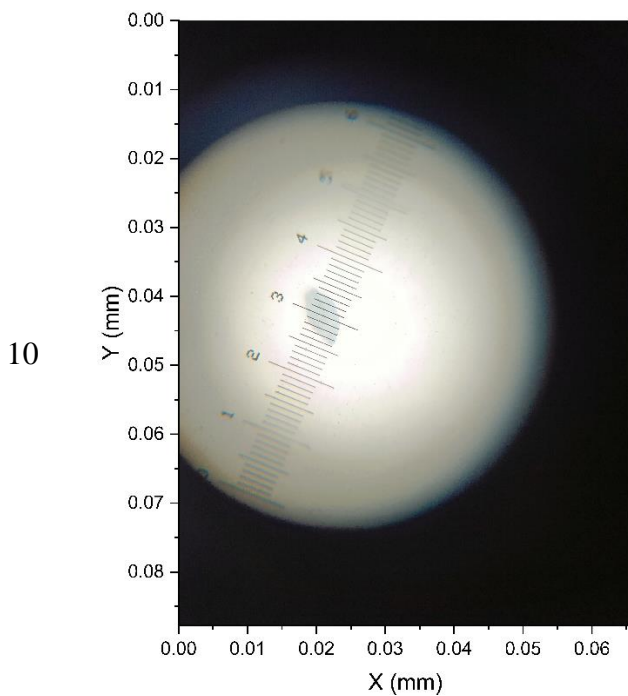
3.7 DIGITAL STATIC CONE PENETRATION TEST

During site inspection and laboratory study, a digital static cone penetrometer test (DSCPT) is an inexpensive way to assess the penetration resistance of granular materials. The cone tip was hydraulically driven at a steady rate of penetration into the ground at a DSCPT location. Both the resistance to sleeve friction and the resistance at the cone tip

21

were measured. The friction in the sleeve and the resistance at the cone tip were measured. The two push handles on the DSCPT, which is employed in the current investigation, are used to manually push the cone into the ground. As shown in Fig. 9, the assembly is made up of a load cell with a 300 kg weight capacity, an LVDT with a 0-20 cm range, a driving rod (1.6 cm in diameter and 49.8 cm long), a cone (60º) at the bottom of the drive rod, and a data-collecting system. Additionally, it shows how the geomaterial and geosynthetics are organised in the steel tank. The top 150 mm of the geomaterial is considered as the subgrade, hence geosynthetics are placed within the subgrade. The 200 mm of geomaterial below is considered as the natural soil.
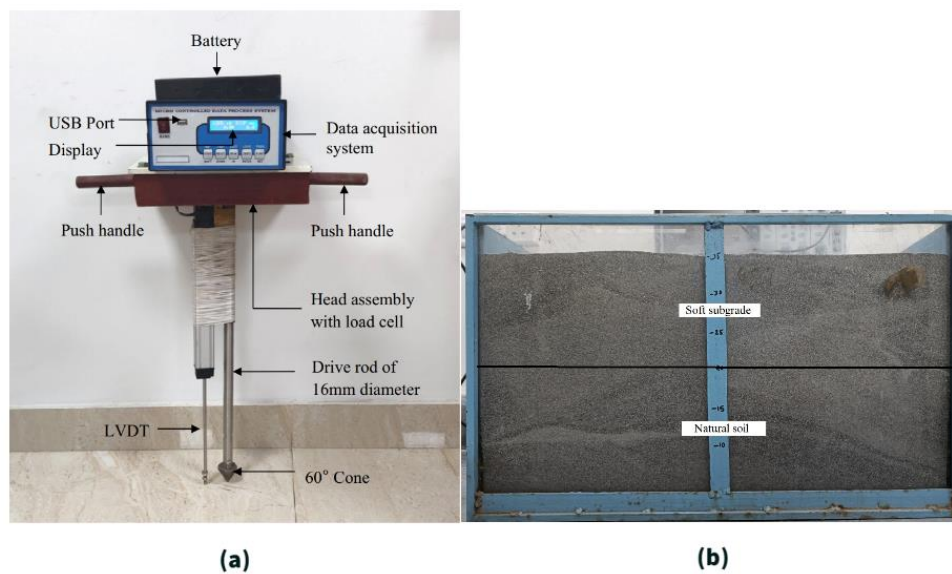
Fig. 9. Figure showing (a) digital static cone penetration test assembly including the steel tank, push handle, 60º cone, drive rod, load cell, LVDT and data acquisition system (Singh et al., 2020) and (b) steel tank filled with geomaterials showing soft subgrade and natural soil.

Body weight exerts a steady strain on the grips, pushing the cone further into the ground. Throughout the tests, the LVDT and load cell were both functional. The load cell assists in monitoring the applied load as the LVDT detects DSCPT penetration. Both deliver the electrical signal, which converts the analogue signal to a digital one, to the data acquisition system. The DSCPT was set up vertically on the granular soil's surface. Since they had an impact on the output data, jerks were to be avoided when pressing the handles of the DSCPT.

The load and displacement data from the load cell and LVDT were automatically stored in a tabular manner in the USB output device. Once the cone stops penetrating into the soil even if the load is increased then the test is completed. The test was conducted on the

sample kept inside a steel tank. The locations at which the test was conducted are shown in Fig. 10. The test was repeated for different layers of reinforcement. The placement of the 50, 100, and 150 mm geogrid reinforcement in every feasible combination has been evaluated.
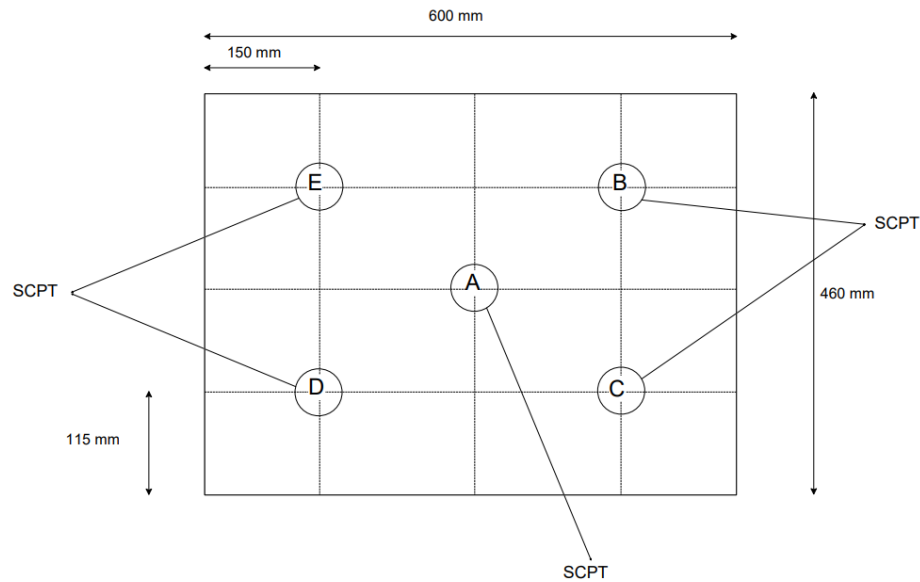
Fig. 10. Layout of locations where digital static cone penetration test was conducted

3.8 GEOSYNTHETIC REINFORCEMENT

Geogrid is used as reinforcement in different layers such as single, double and triple layers. The geogrid is a perforated polypropylene sheet with ribs. It limits the horizontal mobility of the geomaterial which is governed by the coefficient of interface friction. Table 5 is a list of properties of the geogrid that was employed in this investigation. At 0.5 % strain, the geogrid's rigidity, which has a 30×30 mm aperture, is 550 kN/m in the machine direction and 350 kN/m in the cross-machine direction. If the interface friction coefficient between the geomaterial and geosynthetics is high enough, geogrid can stop geomaterial from migrating horizontally when installed at the interface of the subgrade and aggregate layer. The force required to entirely remove a geogrid from the appropriate standard soil was provided by the manufacturer, and it was found to be 1.78 which is the coefficient of interface friction. The geogrid employed in this investigation is depicted in Fig. 11.
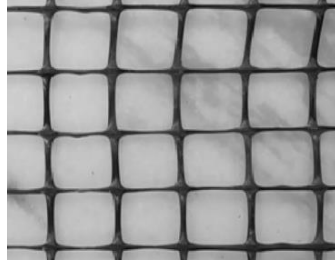
Fig. 11. Geogrid used in the study (Aperture size – 30×30 mm)

Table 5. Properties of geogrid used in the present study (Singh et al., 2020)

Characteristics	Property	Specifications/Magnitude
Physical characteristics	Structure	Bi-axial geogrid
	Colour	Black
	Shape	Quadrangular
	Polymer	Polypropylene
Technical characteristics	Aperture size (mm)	30×30 (MD[a]×CMD[b])
	Stiffness at 0.5 % strain (kN/m)	550×350 (MD[a]×CMD[b])
	Transversal rib width (mm)	2.6
	Longitudinal rib thickness (mm)	3.8
	Junction thickness (mm)	6
Performance characteristics	Aperture coefficient of friction	1.78[c] and 1.14[d]
	Installation damage factor	1

[a] machine direction
[b] cross-machine direction
[c] 10kPa
[d] 20 kPa

3.9 NUMERICAL SIMULATION

A numerical strategy that provides approximate answers to problems in the field is the finite element technique. Partial differential equations with solutions that satisfy the boundary conditions are used to solve issues. Finite element analysis, on the other hand, merely seeks to approximate the field quantity by piecewise interpolation. To mimic the behaviour of geomaterial under dynamic loading, the finite element technique

24

methodology should be used. Software called Abaqus has been used to carry out numerical analysis.

3.9.1 Modeling Assembly

Abaqus 2017 was used to model a 600×350 mm confined tank filled with geomaterial in 2D as shown in Fig 12.
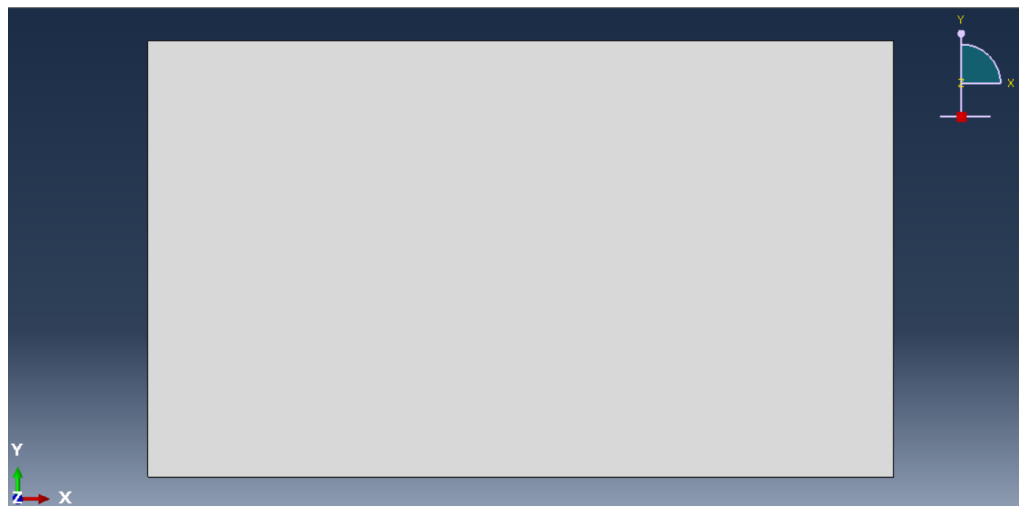
Fig. 12. Model of a confined tank filled with geomaterial.

The Poisson's ratio, Young's modulus, dilation angle, friction angle, and the unit weight of the geomaterial are the input properties adopted in the present study as listed in Table 6.

Table 6. Properties of geomaterial adopted in the present study for performing the finite element simulations

Property	Magnitude
Poisson's ratio, μ	0.45
Young's modulus, E (MPa)	30 - 50
Dilation angle, ψ	1°
Friction angle, ϕ	35°
Unit weight, γ (kN/m3)	16 - 22

3.9.2 Loading Module

Load Application: A vibratory load is applied on the confined tank with geomaterial. The loading is applied according to the load applied by the armature of the electro-dynamic shaking unit used for the experiment. The pressure of the load applied was 30 kPa. The dynamic load was applied at different frequencies such as 5, 10, 15, 20 and 25 Hz as dynamic implicit loads. Fig 13 shows the loading condition on the confined tank filled with geomaterial.
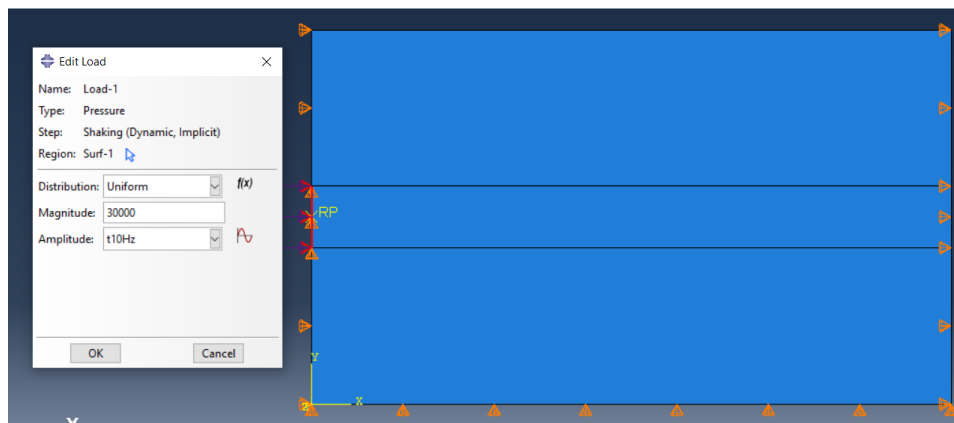
Fig. 13. Loading condition on the model

Boundary Conditions: The fundamental values of variables like velocity, displacement, rotation, etc. at model nodes are specified using the boundary conditions in the numerical model. Additionally, it has been applied to limit the mobility of boundary faces. For the present study, a displacement boundary condition was provided. A displacement/rotation boundary condition specifies the displacement or rotation for each specified degree of freedom or limits the movement of the selected degrees of freedom to zero. Here three such boundary conditions are used to provide confinement to the geomaterials, which are as follows:

1. The bottom of the geomaterial is confined against the vertical motion, $U_2 = 0$ as shown in Fig. 14 (a).
2. The partition where pressure is applied is restricted to move in the vertical direction, $U_2 = 0$ as shown in Fig. 14 (b).
3. Both sides of the geomaterial are confined against the horizontal movement, $U_1 = 0$ as shown in Fig. 14 (c). The pink dots indicate that the selected points are excluded from the applied boundary condition
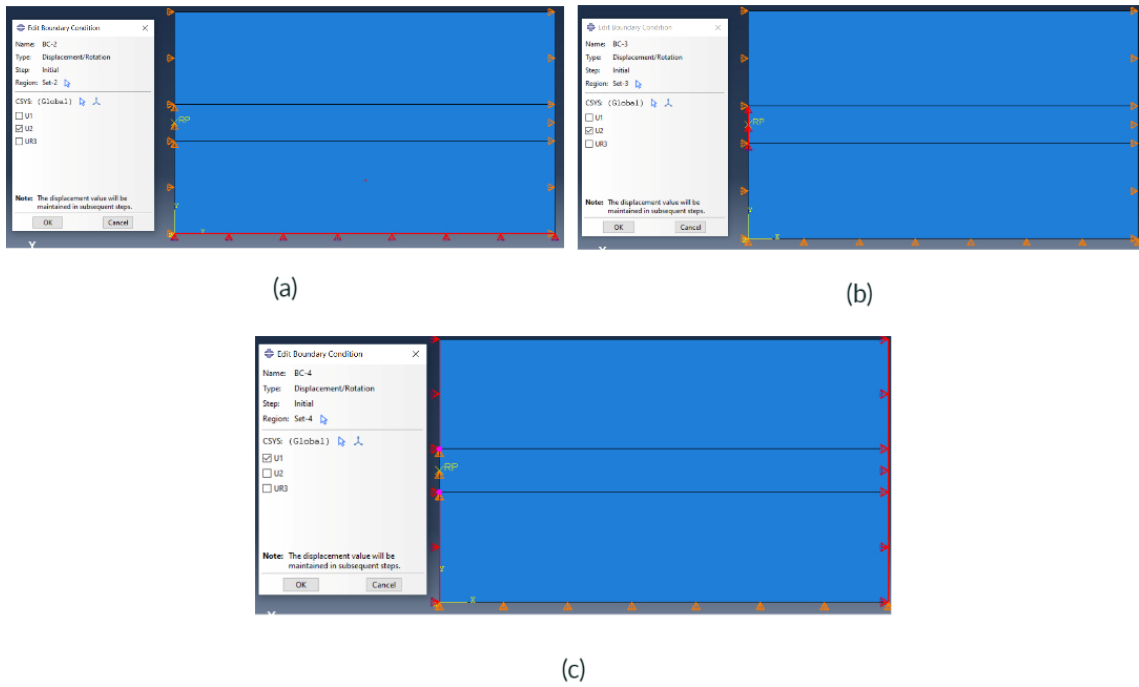
Fig. 14. Boundary conditions of the model (a) $U_2 = 0$, (b) $U_2 = 0$, and (c) $U_1 = 0$

3.9.3 Meshing Module

A key component of Finite Element Analysis (FEA) is meshing, which is the discretization of huge, complicated geometries into a collection of simple, linked elements. Simply said, finite elements are used to break down complicated structures into smaller, simpler shapes. It is crucial to understand how to produce an adequate mesh since mesh size, element type, and element quality all have a direct impact on the accuracy and dependability of an FEA simulation. The different meshing procedures provide varying degrees of automation and user control are:

1. Structured meshing
2. Free meshing
3. Swept meshing

The meshing technique used in the present study is global meshing. The 600×350 mm confined geomaterial is divided into 2100 elements. The size of each element is 10×10 mm as shown in Fig. 15.
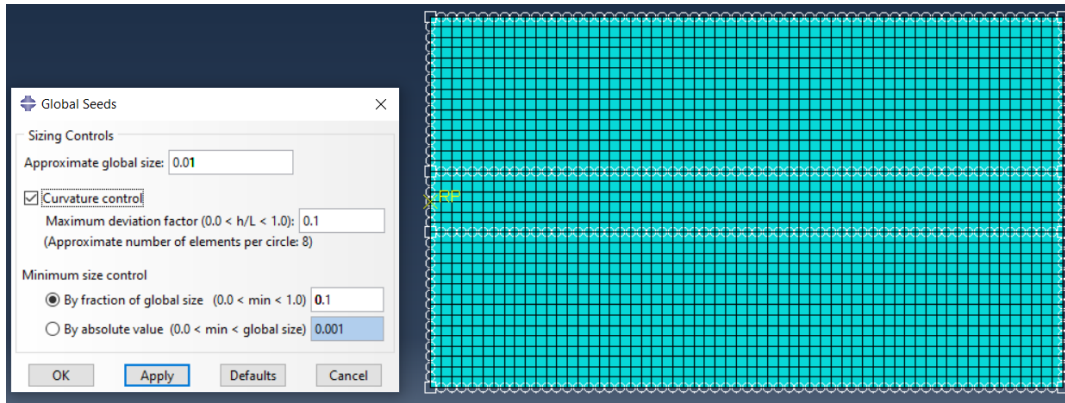
Fig. 15. The meshing of the model

3.9.4 Step Module

Within a model, the sequencing of one or more analytical stages is described. The step sequence provides a simple method for documenting adjustments to the loading of the model and boundary conditions, adjustments to how its constituent parts interact with one another, removal or addition of constituent parts, and any other adjustments that could be made throughout the study. Additionally, it can offer the choice to change the analysis procedure, the data output, and a variety of settings. The present model, which consists of direct integration dynamic analysis for the nonlinear behaviour of the geomaterial, has been simulated using a dynamic implicit scheme as shown in Fig. 16. The D'Alembert principle has been used to measure the displacement, and the motion equation is

$$m\ddot{x} + c\dot{x} + kx = P(t) \tag{3}$$

where P(t) is the loading excitation, m is the system's mass, c and k are the geomaterial's damping coefficient and stiffness constant, and $\ddot{x}, \dot{x}$ and x are the acceleration, velocity and displacement.
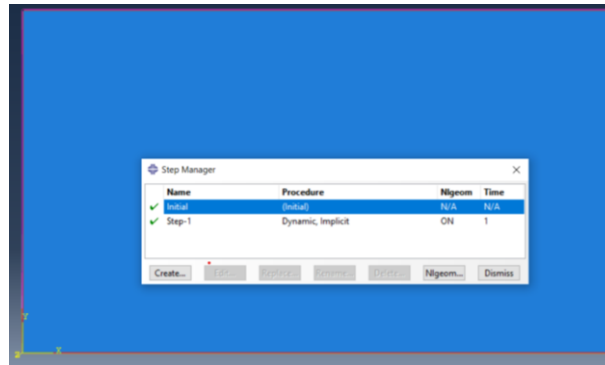
Fig. 16. Steps used in the model

3.10 EXPERIMENTAL SETUP

A steel tank measuring $600 \times 460 \times 400$ mm was filled with geomaterial to verify the depth and displacement change with the frequency that had been anticipated analytically. A steel cylinder, granular substance, dynamic vibrator, data recorder, and accelerometer were all included in the testing configuration. Accelerometers are electromechanical sensors that produce electrical charges proportional to the force exerted upon them. They can be mounted on any surface at any orientation. When the vibrator strikes the tank, the accelerometer (NP-3412) measures the displacement, velocity, and acceleration of sand. It was positioned inside the tank at various depths of 50 - 200 mm from the shaking device and was mounted on a steel plate using petro wax adhesive (Model 080A109). Accelerometer signals are measured using a data acquisition system that logs the static and dynamic activities. While the accelerometer collects the data, the vibrator was excited at 5 - 25 Hz.

Vibrations were produced using an MEV-0020 electro-dynamic vibrator and an MPA-0500 Power amplifier cum signal generator. The electrodynamic vibrator consists of a moving platform which was positioned to hit the steel tank with the geomaterial from the sides as depicted in Fig 17. The accelerometers are positioned at different depths away from the vibrating plate, which will collect the necessary data from the locations. The displacement data was logged by an MVM-555 digital vibration meter.

29
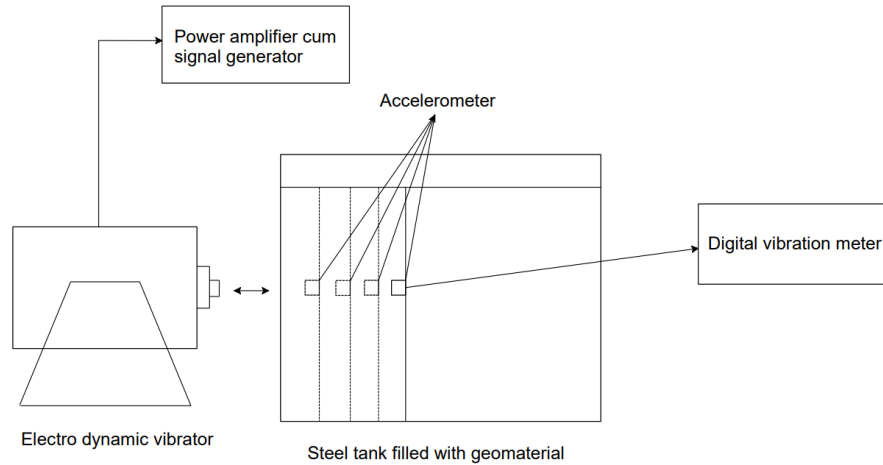
Fig. 17. Diagrammatic representation of the experimental setup showing the arrangement of accelerometer along with power amplifier cum signal generator, electrodynamic vibratory shaker, a steel tank filled with geomaterial, and digital vibration meter.

3.11 MACHINE LEARNING APPROACH

Data Collection - Gather data related to confined geomaterial, such as tank width, D_{50}, density, armature-applied pressure, loading frequency, and displacement. Ensure that the data contains multiple input variables.

Data Pre-processing - Normalize the input variables to clean the dataset, making it suitable for training a machine learning model.

Feature Selection - Determine the input variables that have an impact on the displacement of confined geomaterial under vibratory load. These variables may include tank width, D_{50}, density, armature-applied pressure, and loading frequency.

Model Selection - Choose a machine learning algorithm based on the characteristics of the input parameters and their connection to the target variable.

Model Training - Divide the dataset into a training set and a testing set. Train the selected machine learning model using the input and target variables from the training set. This process enhances the model's ability to identify correlations and patterns within the data.

Model Evaluation - he trained model is evaluated using the testing set. The accuracy of displacement prediction by the models can be measured using various metrics, including mean squared error (MSE), root mean squared error (RMSE), mean absolute error

30

(MAE), and coefficient of determination (R^2). These metrics, R^2, RMSE, MAE, and MSE, are calculated using equations (4-7) (Ahmad et al., 2018; Younas et al., 2022; Ibrahim et al., 2022).

$$R = \frac{n \sum(xy) - (\sum x)(\sum y)}{\sqrt{(n \sum x^2 - (\sum x)^2)(n \sum y^2 - (\sum y)^2)}} \tag{4}$$

$$RMSE = \sqrt{\frac{\sum_{i=1}^{n}(y_i - \hat{y}_i)^2}{n}} \tag{5}$$

$$MAE = \frac{1}{n} \sum_{i=1}^{n} |\hat{y}_i - y_i| \tag{6}$$

$$MSE = \frac{1}{n} \sum_{i=1}^{n} (y_i - \hat{y}_i)^2 \tag{7}$$

the variables x and y represent the input and output parameters, respectively, for a dataset consisting of n sample points. The predicted values of the output parameter are denoted as $\hat{y}_i$, while the actual values are represented by y_i.

Prediction - Once the model has been trained and evaluated, it can be employed to predict or forecast displacement for untested samples. By providing the relevant sand parameters as input to the trained model, it will generate estimates of displacement. These estimates serve as predictions for the unknown samples based on the patterns and correlations learned during the training process.

3.11.1 Machine Learning Models
Decision Tree

The Decision Tree (DT) classifier categorizes an unknown sample by iteratively applying one or more decision functions, as described by Swain and Hauska (1977). It takes the form of a tree structure, where the leaf nodes indicate classification outcomes, and the internal nodes represent dataset features, branching, and decision-making processes. By utilizing dataset features, the DT approach determines the appropriate test or decision at each step. This methodology effectively breaks down complex problems into simpler ones, providing a solution that is easily comprehensible, as highlighted by Xu et al. (2005).

Let $\underline{X}$ represent the pattern or feature vector, and Y represent the class label that has been assigned to $\underline{X}$. $\underline{X}$ takes values from the real-valued space R^q, whereas Y takes integer values. The d(.) decision rule function is in charge of mapping the elements in R^q to the matching class label Y (Safavian and Landgrebe, 1991). true misclassification rate of d is

$$R^*(d) = p\big(d(\underline{X}) \neq Y\big) \tag{8}$$

To train a Decision Tree (DT) model, the process involves utilizing recursive partitioning and multiple regressions on the training dataset. This approach initiates at the root node and continues by iteratively dividing the data at each internal node based on a predefined rule. This splitting process is repeated until specific stopping criteria are met, as described by Rodriguez-Galiano et al. (2015).

Two commonly used scoring criteria for determining the best split at each node are Information Gain (InfoGain) (Quinlan, 1993) and Gini Index (Gini) (Breiman, 1984). These criteria evaluate the impurity or uncertainty of the data at each potential split point and aid in selecting the most informative and discriminative features for decision-making within the DT model.

$$Info = -\sum_j \left(\frac{N_j(t)}{N(t)}\right) \log_2 \left(\frac{N_j(t)}{N(t)}\right) \tag{9}$$

Where N_j is the number of samples belonging to class j, N(t) is the number of samples in node t, and $N_j(t)$ is the number of class j samples in node t.

$$InfoGain = Info(parent) - \sum_k (p_k) Info(child_k) \tag{10}$$

where Info (q) is the information of the feature subspace q, and p_k is the proportion of samples passed to the kth subspace.

$$Impurity = 1 - \sum_j \|p(j)N_j(t)/N(t)\|^2 \tag{11}$$

$$Gini = Impurity(parent) - \sum_k (p_k) Impurity(child_k) \tag{12}$$

In the given context, P(j) represents the prior probability that a sample belongs to class j within a set of training samples. The notation ||g|| signifies the normalization of the vector g to unit length.

To align with the default configuration in the Matlab decision tree code for the micro-array example, proportional priors are utilized. This means that the prior probability p(j) for class j is calculated based on the relative frequency of samples belonging to class j (Nj) compared to the total number of samples in class 1 (N (1)). This normalization helps ensure that the prior probabilities sum up to 1 and provides a consistent reference point for making classification decisions (Myles et al., 2004).

Three alternative DT topologies are accessible in this situation. The first architecture is made up of "Fine" DT, the most sophisticated of the three. The second architecture is called "Medium," while the third is called "Coarse."

Gaussian Process Regression

The vector D = {y(xi): I = 1...n} represents a collection of data points, where x ∈ χ is an arbitrary input variable. Given a test input x*, our goal is to estimate the expected value $\mathbb{E}$ [y(x*) | x*, D] and the covariance cov[y(x*) | x*, D]. The correlations between the components of y(x) can vary as x changes, encompassing both signal and noise.

If we assume x = t, one component of the p-dimensional vector y(t) may indicate the expression level of a particular gene at time t. The remaining components, (t), would reflect the variances and correlations among these genes at time t. Rather than assuming temporal dependence, we model the entire vector y(x) to capture its interactions and dependencies, considering the correlations and interactions among all its components (Wilson et al., 2011).

$$y(x) = W(x)[f(x) + \sigma_f \in] + \sigma_y z \tag{13}$$

∈ represents a random variable, and z represents independent and identically distributed white noise that follows a Gaussian distribution with a mean of 0 and an identity covariance matrix, denoted as N(0, I).

The matrix W(x) is a p×q matrix composed of independent Gaussian processes (GPs). Each element of W(x) is a GP, and they are mutually independent. On the other hand, the

vector f(x) = (f1(x), ..., fq(x))^T is a q×1 vector composed of independent GPs. Similarly, each element of the vector f(x) is a GP, and they are also mutually independent (Quinonero-Candela and Rasmussen, 2005).

A Gaussian Process (GP) refers to a collection of random variables that have joint Gaussian distributions, and this property holds for any finite number of variables. Various types of Gaussian Process Regression (GPR) models exist, including the Matérn 5/2 GPR, rational quadratic GPR, squared exponential GPR, and exponential GPR.

The rational quadratic GPR kernel is particularly useful when dealing with data that exhibits fluctuations at different scales. This method finds applications in image analysis, machine learning, geostatistics, spatial statistics, and multivariate statistical analysis in metric spaces.

In the context of function space, the squared exponential GPR represents a regression model with an infinite number of basis functions, similar to a radial basis function regression model. The squared Euclidean distance is used to distinguish it from the exponential GPR. One notable characteristic of the squared exponential GPR is the use of kernels to replace inner products of basis functions.

The Matérn 5/2 kernel is derived by taking Fourier transforms of the Radial Basis Function (RBF) kernel using spectral densities of the stationary kernel. The Matérn 5/2 kernel addresses the issue of high-dimensional concentration of measure and is suitable for modeling data in such spaces.

The exponential GPR employs kernels instead of basis function inner products. While it accurately approximates smooth functions, it may struggle to detect abrupt discontinuities in data.

These descriptions highlight the characteristics and applications of different GPR models, based on their respective kernel functions.

Ensemble

Ensemble machine learning is a technique that combines multiple basic models to create a more accurate prediction model. Ensemble classifiers classify new data points by aggregating the predictions of individual models, either through voting with or without

weights, as described by Dietterich (2000). Ensemble methods address various machine learning problems by training multiple models and integrating their predictions to improve overall predictive performance, as highlighted by Sagi and Rokach (2018). These ensemble techniques leverage the diversity and expertise of multiple models to handle complex patterns, mitigate overfitting, and enhance generalization, making them essential in modern machine learning across diverse domains.

Bagging is an ensemble technique that involves averaging the predictions of multiple decision trees, each trained on different subsamples of the same dataset. This approach aims to improve prediction accuracy by reducing variance through the combination of multiple models.

Boosting, on the other hand, focuses on sequentially adding ensemble members that correct the predictions made by previous models. It produces a weighted average of the predictions and emphasizes the samples that were incorrectly classified by adjusting sample weights. By iteratively updating the sample weights and integrating the outputs of multiple models, boosting enhances the classification capabilities of the basic models, as explained by Dong et al. (2020).

In the specific experiment mentioned, the Classification Toolbox in MATLAB was used. The study involved constructing decision tree structures of different sizes, namely fine and medium, as well as utilizing the Matérn 5/2 GPR, rational quadratic GPR, squared exponential GPR, exponential GPR, and boosted tree models. These models were employed to predict soil displacement when subjected to vibratory pressure.

CHAPTER 4

RESULTS AND DISCUSSION

4.1 BASIC PROPERTIES OF SOIL

The geomaterial is sand that has been poorly graded (SP), according to the grain size distribution curve. There are values for the uniformity (C_u) and curvature (C_c) coefficients are 2.86 and 1.07, respectively (before cleaning) and 2.31 and 0.9423, respectively (after cleaning). The shear stress vs. normal stress graph displays cohesiveness and the angle of internal friction. The compaction curve gives the optimum moisture content and maximum dry density. Table 7 displays the basic properties of geomaterial before and after cleaning.

Table 7. Basic properties of the geomaterial

Properties	Magnitude (Before cleaning)	Magnitude (After cleaning)
Material	Poorly graded sand (SP)	Poorly graded sand (SP)
Specific gravity	2.74	2.68
Optimum moisture content, OMC (%)	4.9	10.4
Maximum dry density, MDD (kN/m³)	16.56	17
Cohesion, c (kPa)	9.47	4.4
Friction angle, ϕ	34.27	36.59º

4.2 DIGITAL STATIC CONE PENETRATION LAB TEST

DSCPT was conducted on geomaterial at five test locations namely A, B, C, D and E. When the driving rod is positioned near the top of the geomaterial, the cone has been

shown to penetrate quite a distance on its own. Since the geomaterial is soft, it did not resist the cone against penetration. As we can see from the graph that the cone penetrated up to 87 and 89 mm at test locations A and B respectively without the application of load for unreinforced subgrade. There are four cases in which DSCPT was conducted. They are as follows:

i.   Without reinforcement

ii.   Single layer of reinforcement

iii. Double layer of reinforcement

iv.   Triple layer of reinforcement

When no reinforcement was placed the cone sinks into the geomaterial without any resistance due to its self-weight. After a certain depth, the densification of soil due to overburden pressure made the geomaterial achieve a certain amount of strength. The load-displacement curves show that geogrid reinforcement offers higher resistance against penetration in the geomaterial. Using this device, a penetration depth of 180 mm corresponding resistance has been increased. The curve for locations B, C, D and E are in conjunction, hence only one location (B) is represented in the Fig. 19, 21, 23, and 25.

4.3 INFLUENCE OF GEOGRID REINFORCEMENT

The characteristics of geogrid reinforcement, the thickness of subgrade, the performance of geogrid at its interface with the geomaterial, the location of the geogrid, the number of geogrid layers, etc., are taken into consideration in the present study for analysing the effectiveness of geogrid-reinforced unpaved roads. The presence of geogrid reinforcement has had an impact on the strengthening of the geomaterial. This study has been conducted for obtaining optimum the number of layers and the location of the geogrid.

4.2.1 Single-layer Geogrid Reinforcement

When only one reinforcement layer is taken into account, the geogrid reinforcement installed at 50 mm from the surface of the geomaterial performed better than that placed at 100 and 150 mm from the surface. While considering the load-displacement behaviour at test location A as shown in Fig. 18, the cone is penetrating up to a depth of 57 mm

without any load. This is due to the densification of geomaterial beneath the geogrid reinforcement. After this point, the geogrid reinforcement provides a reinforcement effect by providing additional strength to the geomaterial. When test location B as shown in Fig. 19 is considered, the cone is penetrating without any load up to a depth of 66 mm. Here boundary effect is predominant, due to which a slight change in the behaviour compared to location A is taking place.

Fig. 18. Load-displacement curve for single layer geogrid-reinforced and unreinforced systems derived from DSCPT data at test location A
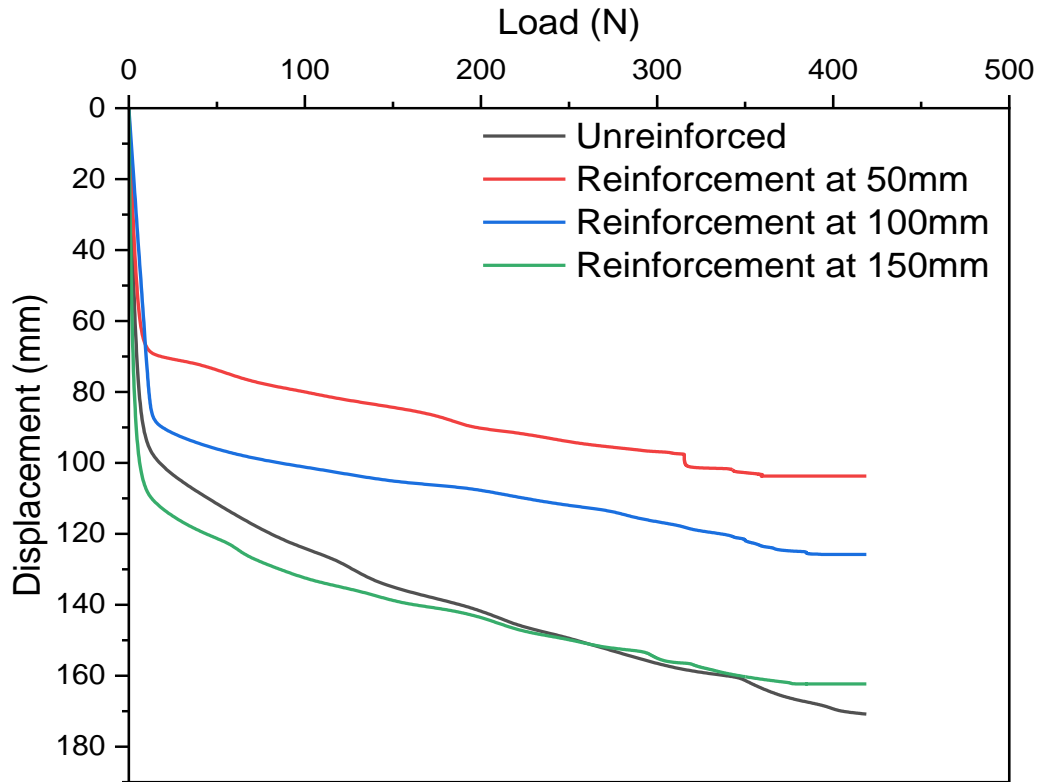
Fig. 19. Load-displacement curve for single layer geogrid-reinforced and unreinforced systems derived from DSCPT data at test location B

4.2.2 Double-layered Geogrid Reinforcement

The double layered is the most efficient among all the cases for location A as shown in Fig. 20. When reinforcement is placed at 50 and 100 mm from the top of the geomaterial, the minimum penetration is obtained compared to all the other combinations. The cone penetrates up to 60 mm without resistance because of the densification effect. After this point reinforcement effect develops which gives strength to the geomaterial. For B, C, D and E locations as shown in Fig. 21 for double-layered geogrid reinforcement, when they are placed at 50 and 150 mm from the top is found to be the most efficient. In this case, the densification effect has been observed upto a depth of 62 mm.

Fig. 20. Load-displacement curve for double layer geogrid-reinforced and unreinforced systems derived from DSCPT data at test location A

Fig. 21 . Load-displacement curve for double layer geogrid-reinforced and unreinforced systems derived from DSCPT data at test location B

4.2.3 Triple-layered Geogrid Reinforcement

The triple-layered is the optimum among all the cases when test locations B, C, D and E are considered as shown in Fig. 23. For these locations, the densification effect has been observed upto 62 mm. For location A as shown in Fig. 22, the reinforcement effect has been initialised at 68 mm. After this point, a reinforcement effect develops which gives strength to the geomaterial.
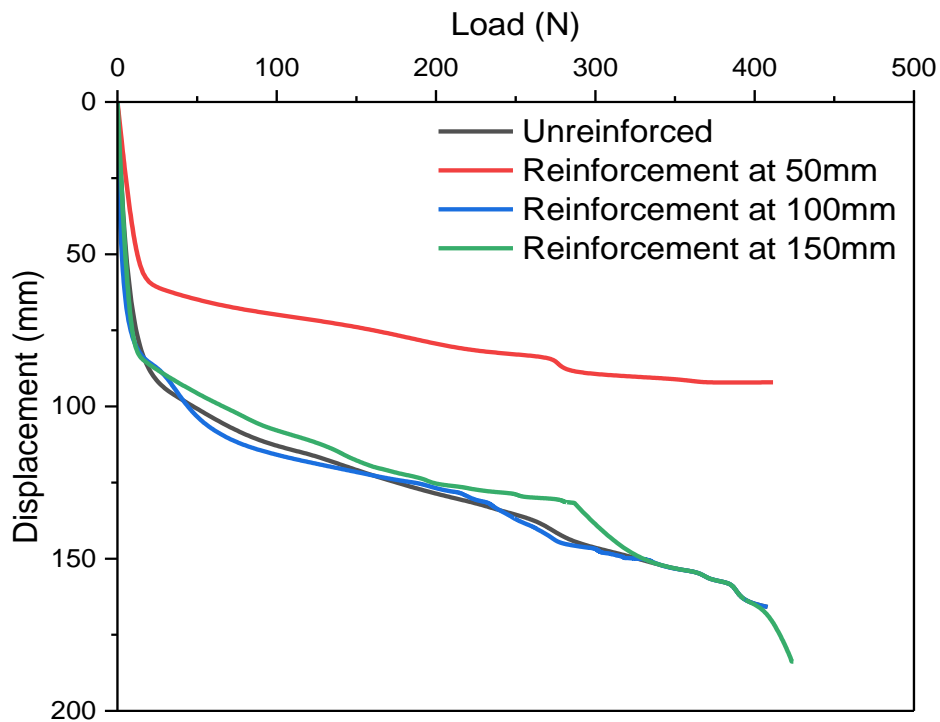

Fig. 22. Load-displacement curve for triple layer geogrid-reinforced and unreinforced systems derived from DSCPT data at test location A
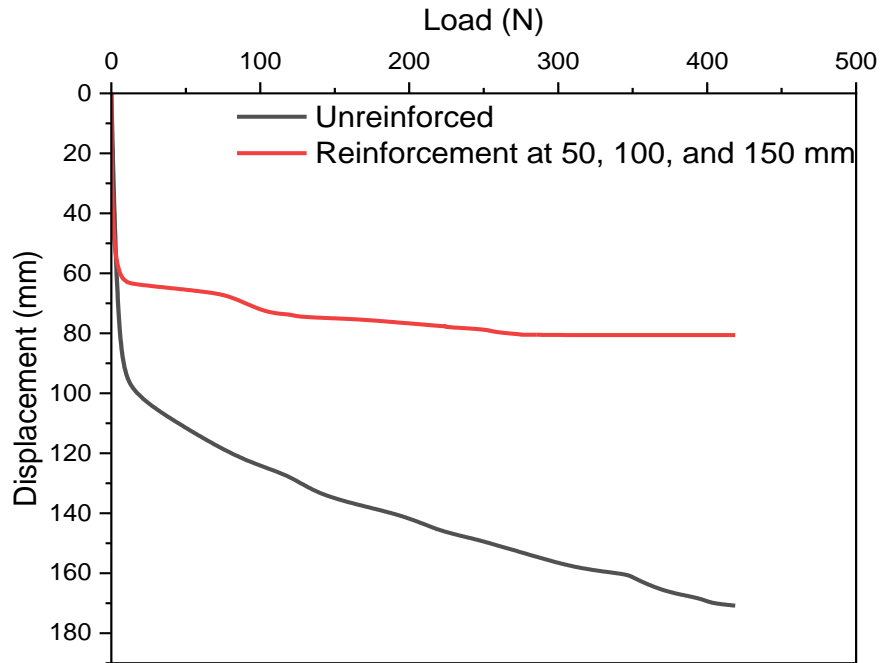
Fig. 23. Load-displacement curve for triple layer geogrid-reinforced and unreinforced systems derived from DSCPT data at test location B

Because of the boundary effect caused by the confinement from the steel tank, the outcomes of locations A as shown in Fig. 24 and B as shown in Fig. 25 are different. The side walls of the steel tank prevent the geomaterial from moving laterally. The boundary effect has been given due consideration while conducting the DSCPT for locations B, C, D and E. For situations where the boundary effect is significant, triple-layered geogrid reinforcement can be used. The kerbs used in paved roads can act as boundaries and for other situations like unpaved roads, double layered reinforcement.
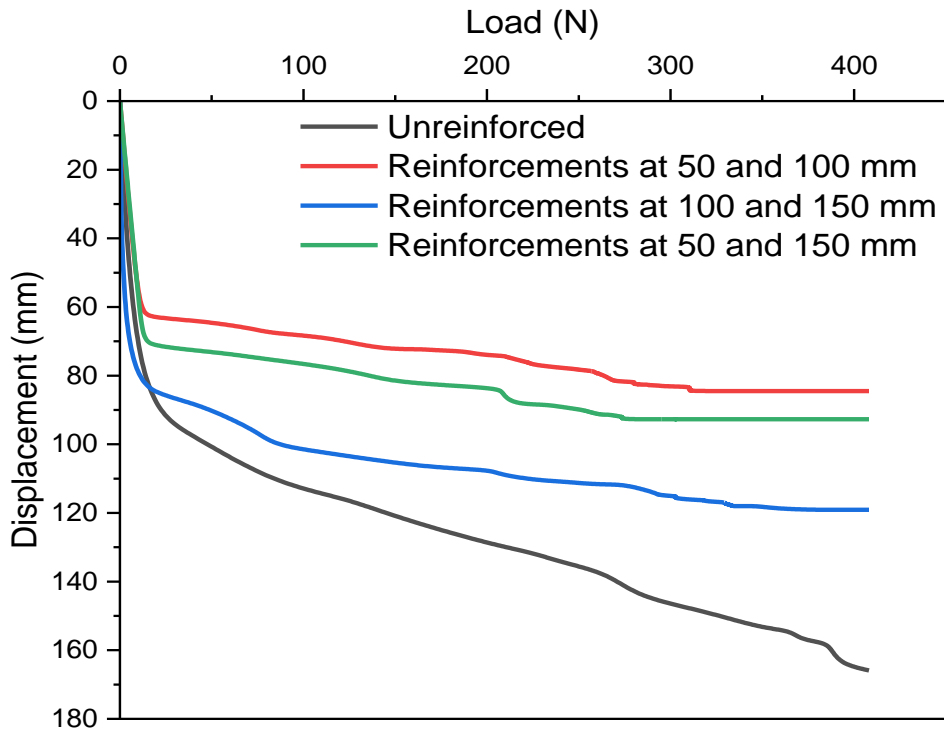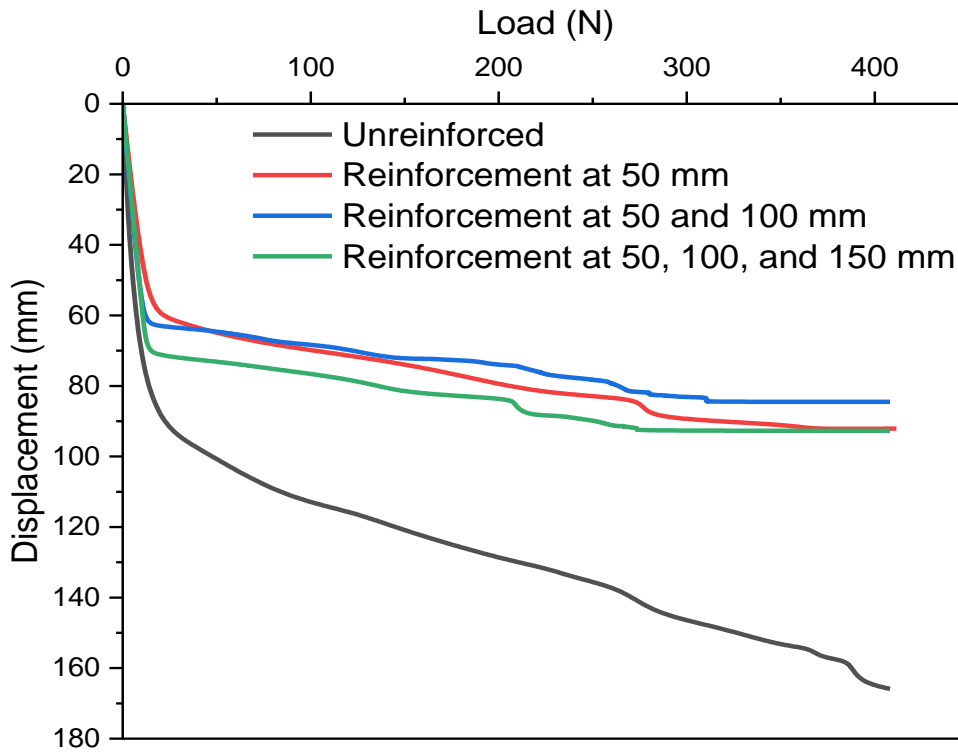
Fig. 24. Load-displacement curve for single, double, and triple layer geogrid-reinforced and unreinforced systems derived from DSCPT data at test location A
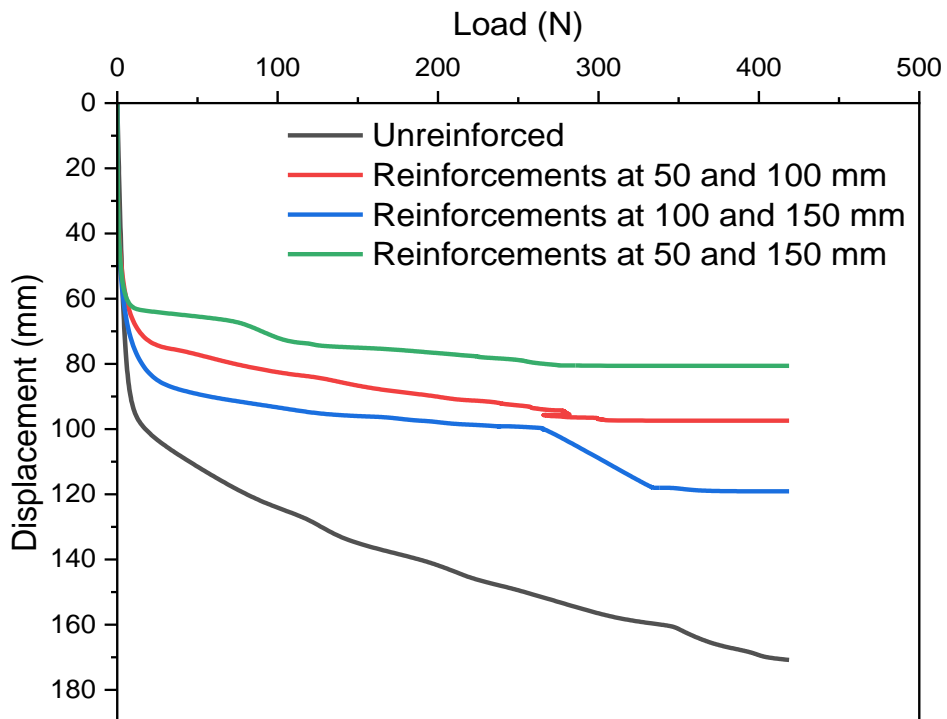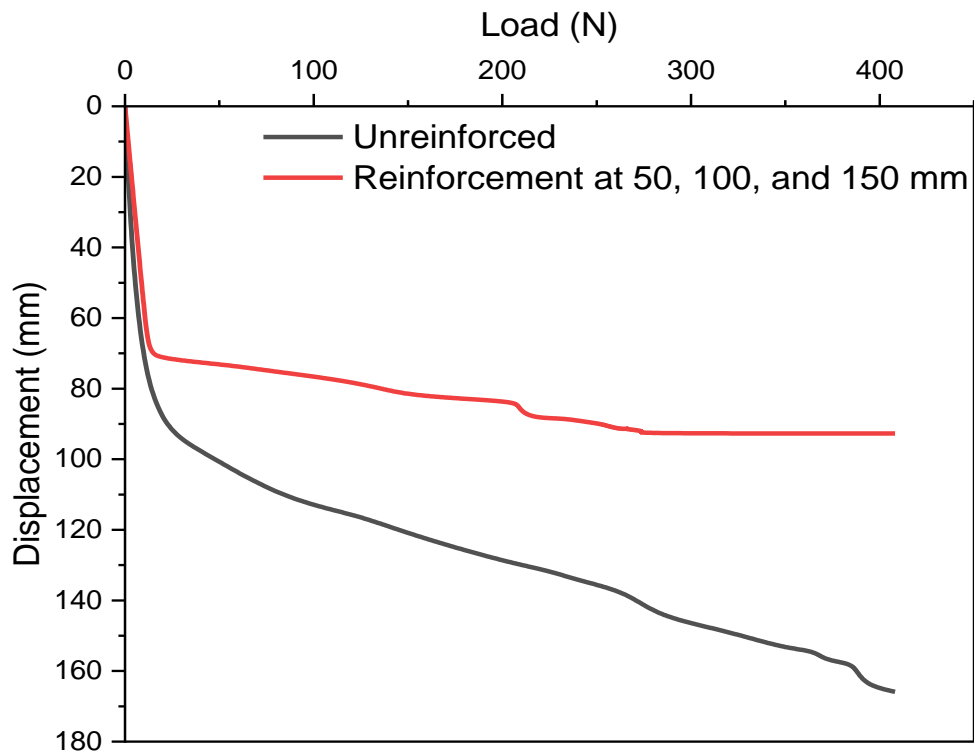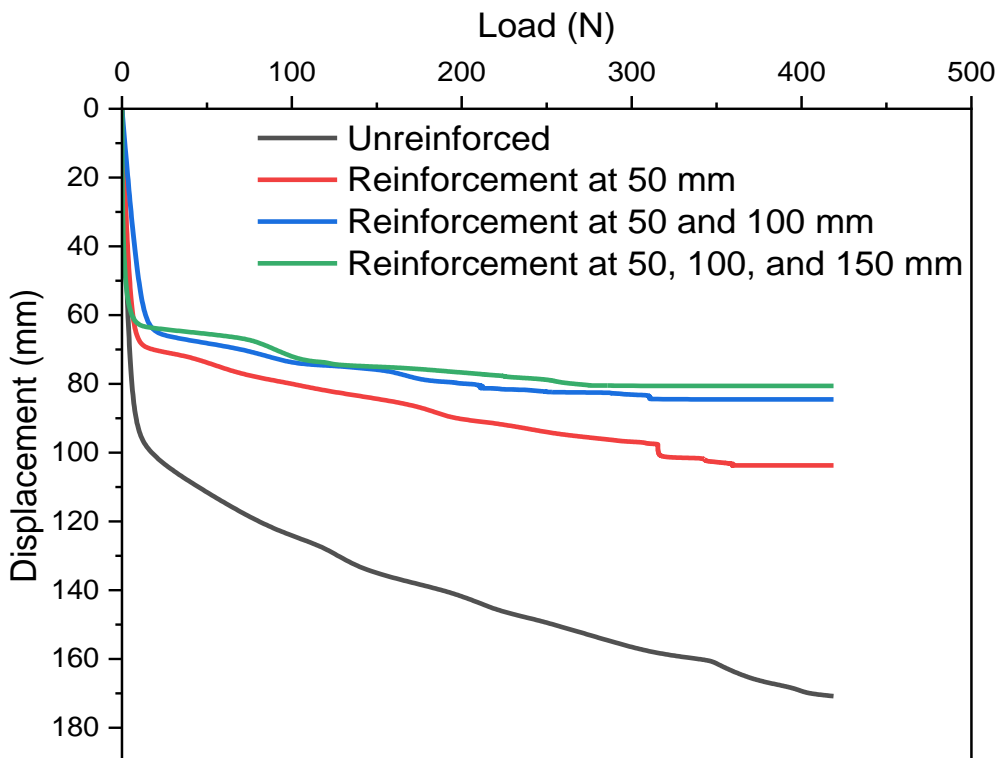

Fig. 25. Load-displacement curve for single, double, and triple layer geogrid-reinforced and unreinforced systems derived from DSCPT data at test location B

4.3 NUMERICAL SIMULATION AND EXPERIMENTAL SETUP

The outcomes of the experiment and the numerical forecast are contrasted for varied input parameters considered in the study. To record the dynamic reaction of the geomaterial, the accelerometers are positioned at various distances from the shaking equipment. As the waves move away from the vibratory source, the displacement should be decreasing. The test findings produced an outcome that was acceptable when compared to the numerical modelling. The findings are displayed in the figures below as shown in Fig. 27.

When densities are examined, the geomaterial does not exhibit a significant variation in displacement because of compression. The geomaterial is unable to move easily with the armature frequency that it strikes the tank due to containment and compaction. The change of displacement at different frequencies spanning from 5 to 25 Hz is depicted in the accompanying figure as shown in Fig. 28. As frequency rises, the displacement tends to grow, and as depth rises, it tends to diminish. The deformed soil mesh after the application of excitation load is shown in Fig. 26.
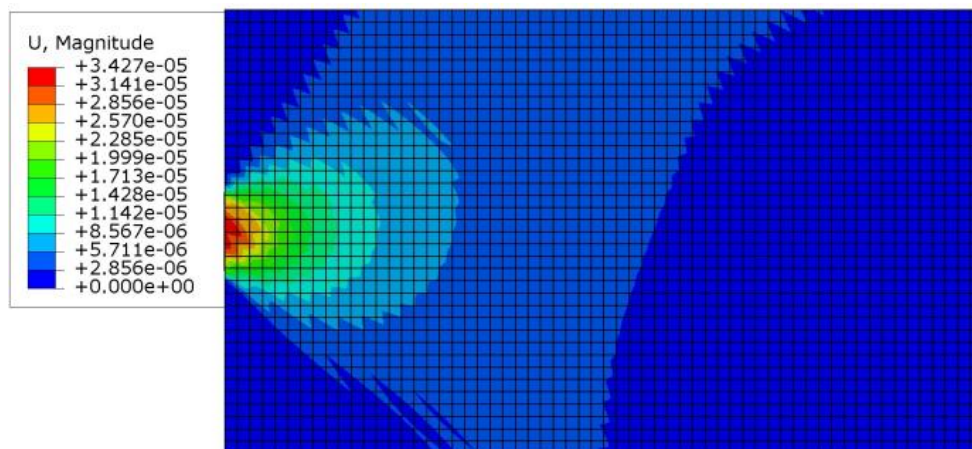
Fig. 26. Deformed soil mesh near the applied excitation, in total displacement direction
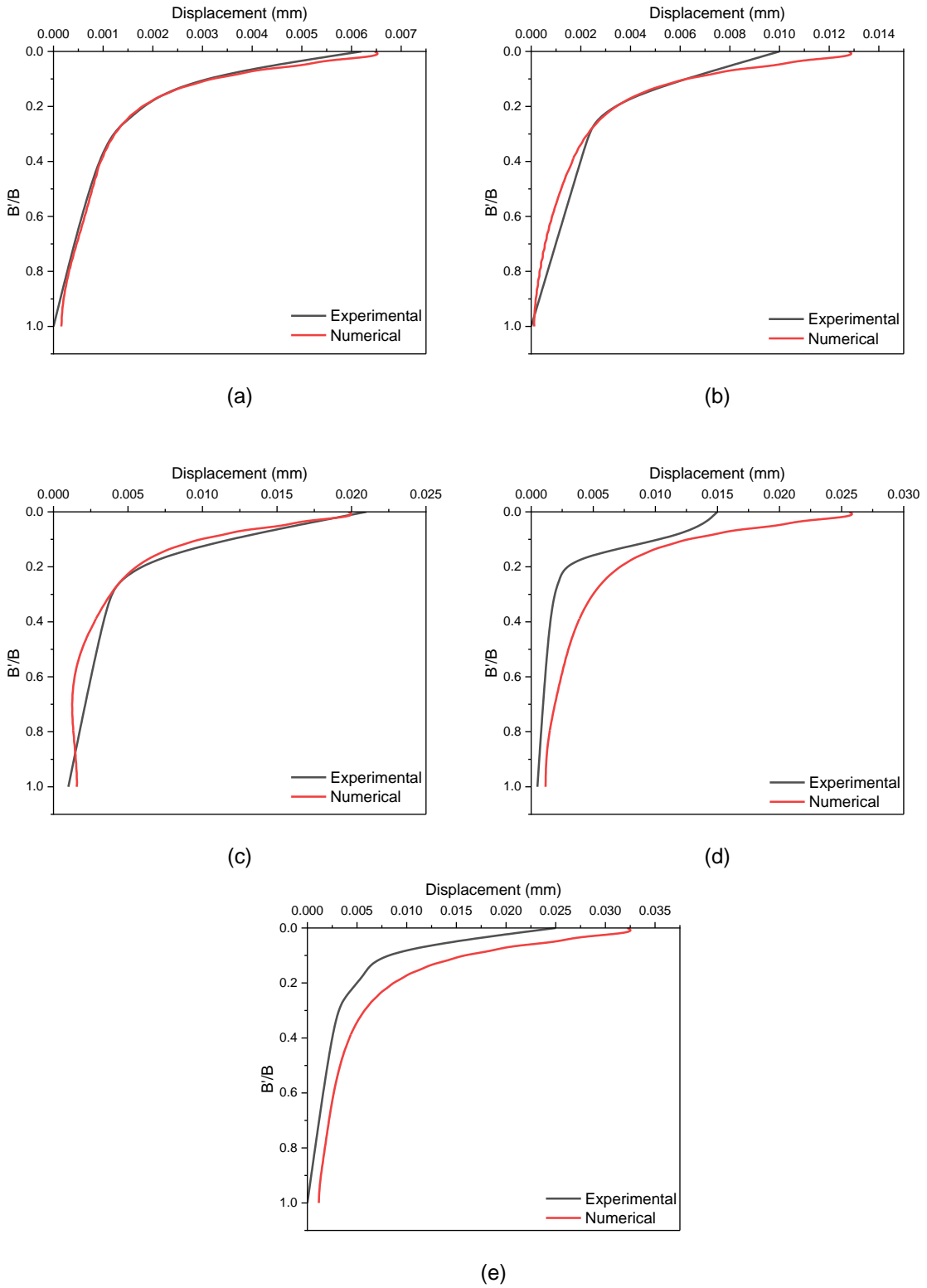
Fig. 27. Comparison of experimental and numerical results on displacement variation along depth ratio at frequencies of (a) 5 Hz, (b) 10 Hz, (c) 15 Hz, (d) 20 Hz, and (e) 25 Hz
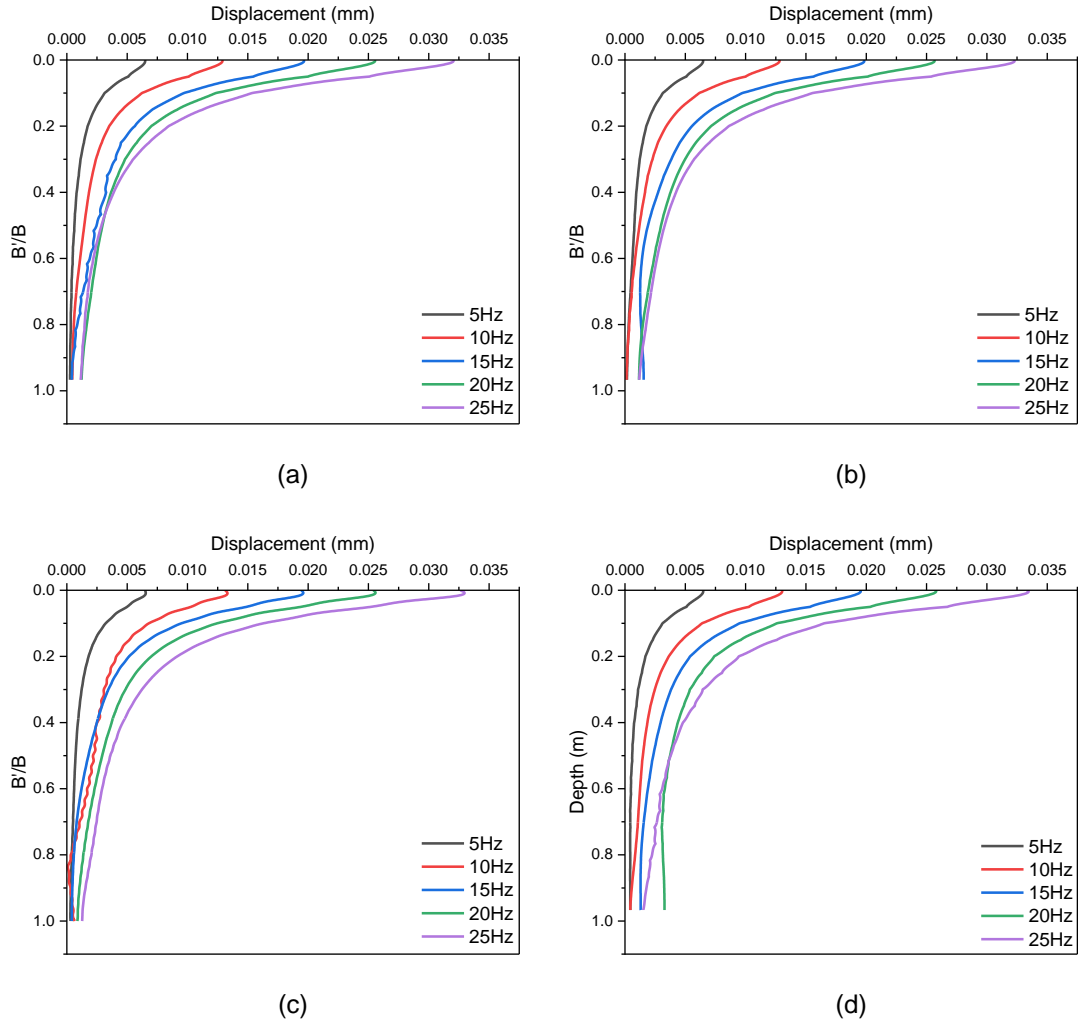
Fig. 28. The variation of displacement along the depth ratio for the 5 to 25 Hz frequency range at (a) $\gamma =$ 16 kN/m^3, (b) $\gamma = 18$ kN/m^3, (c) $\gamma = 20$ kN/m^3, and (d) $\gamma = 22$ kN/m^3

The numerical and experimental findings are in great conjunction for confined geomaterial subjected to vibratory load for various input parameters considered in the study. When the frequency is increased the values move apart from each other.

The shear stress (τ) which is a function of depth (z) may be calculated using an equation:

$$\tau = \int_0^z \rho \ddot{u} dz \tag{14}$$

Here ρ is the density and $\ddot{u}$ is the acceleration.

Also, shear strain can be calculated as:

$$\gamma(z_i) = \left[(u_{i+1} - u_i)\frac{(z_i - z_{i-1})}{(z_{i+1} - z_i)} + (u_i - u_{i-1})\frac{(z_{i+1} - z_i)}{(z_i - z_{i-1})}\right]/(z_{i+1} - z_{i-1}) \qquad (15)$$

where z is depth and u are the displacement.

Further explaination of the equation (4) and (5) is available in Zeghal and Elgamal (1994). Shear modulus can be calculated by showing shear stress and strain after they have been acquired. The slope of the loop gives the shear modulus (G). Fig. 29 and 30 depict the fluctuation of the shear stress-strain hysteresis loop at various frequencies (50 and 75 Hz) and different Young's moduli (30- 50 MPa).
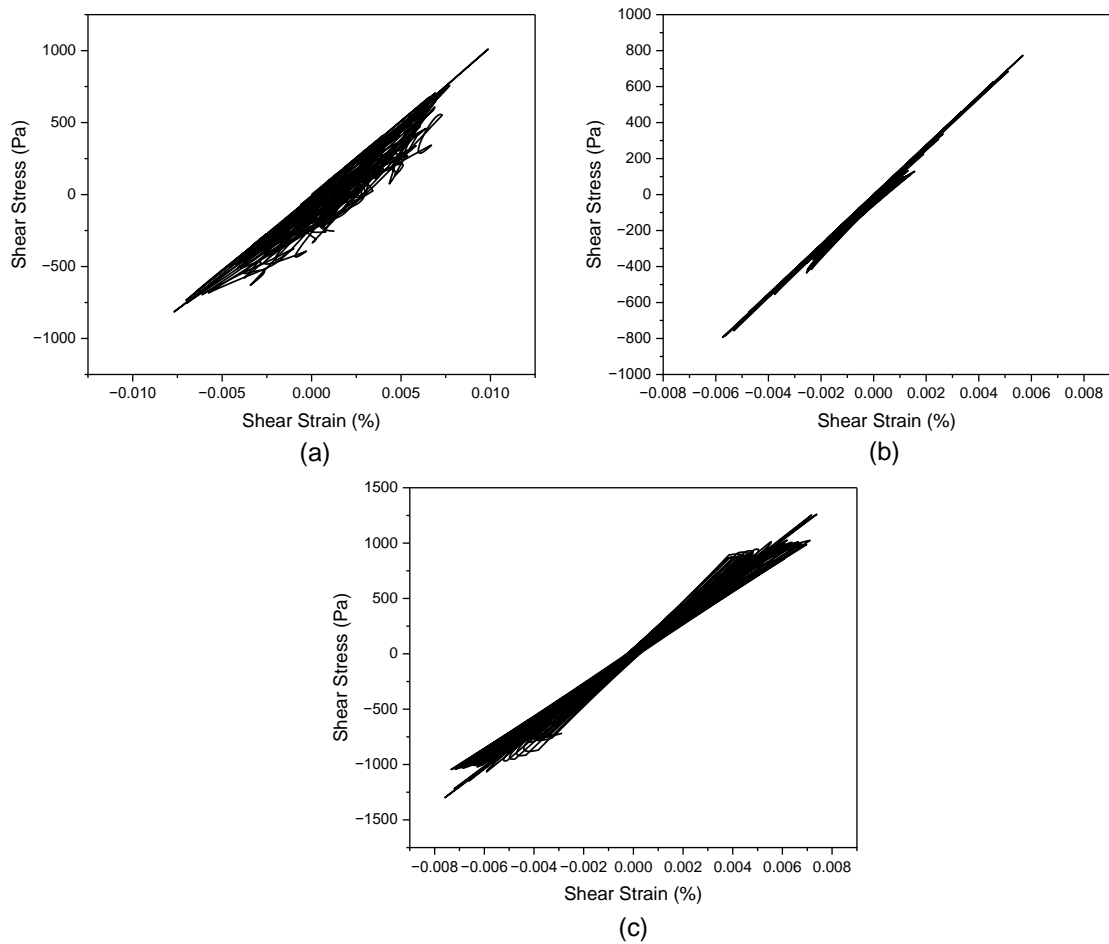
Figure 29. Shear stress-strain hysteresis loop at 50 Hz frequency when (a) E = 30 MPa, (b) E = 40 MPa, and (c) E = 50 MPa
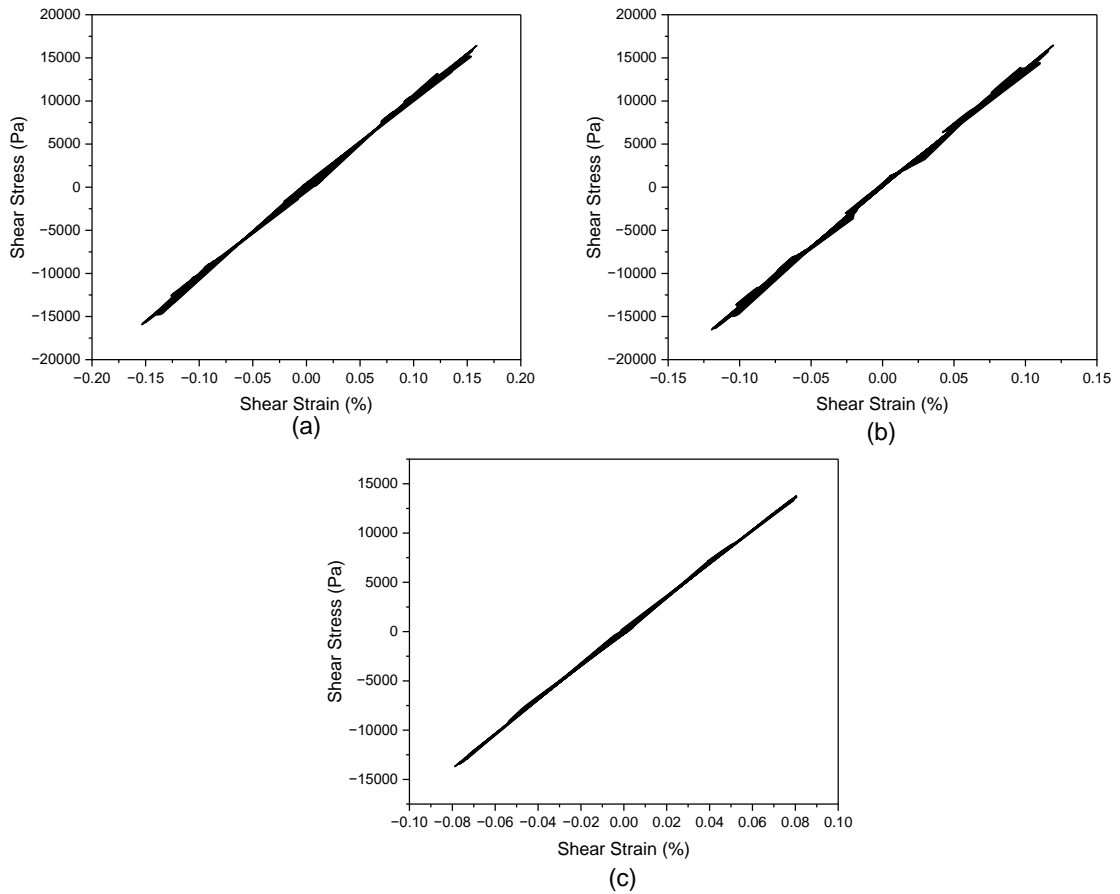
Fig. 30. Shear stress-strain hysteresis loop at 75 Hz frequency when (a) E = 30 MPa, (b) E = 40 MPa, and (c) E = 50 MPa

The shear stiffness of the geomaterial was calculated by determining the slope of the curve from the shear stress-strain hysteresis loop. The shear modulus value stays constant since the loops are so close to one another. Additionally, it was shown that it does not alter often with frequency variation. But there is a change while varying Young`s modulus. Young's moduli of 30, 40, and 50 MPa, respectively, correspond to shear moduli of 9, 10, and 20 MPa.

The damping can be calculated using the logarithmic decrement method. It is known that the effect of damping decreases the amplitude of vibration with time. If x_n and x_{n+1} are the two successive peak displacements then,

$$\delta = ln\left(\frac{x_n}{x_{n+1}}\right) = \frac{2\pi D}{\sqrt{1 - D^2}} \qquad (16)$$

where δ is the logarithmic decrement and D is the damping ratio as given in Das and Luo (2016). The damping ratio's relationship to shear strain at various densities and frequencies is shown in Fig. 31.
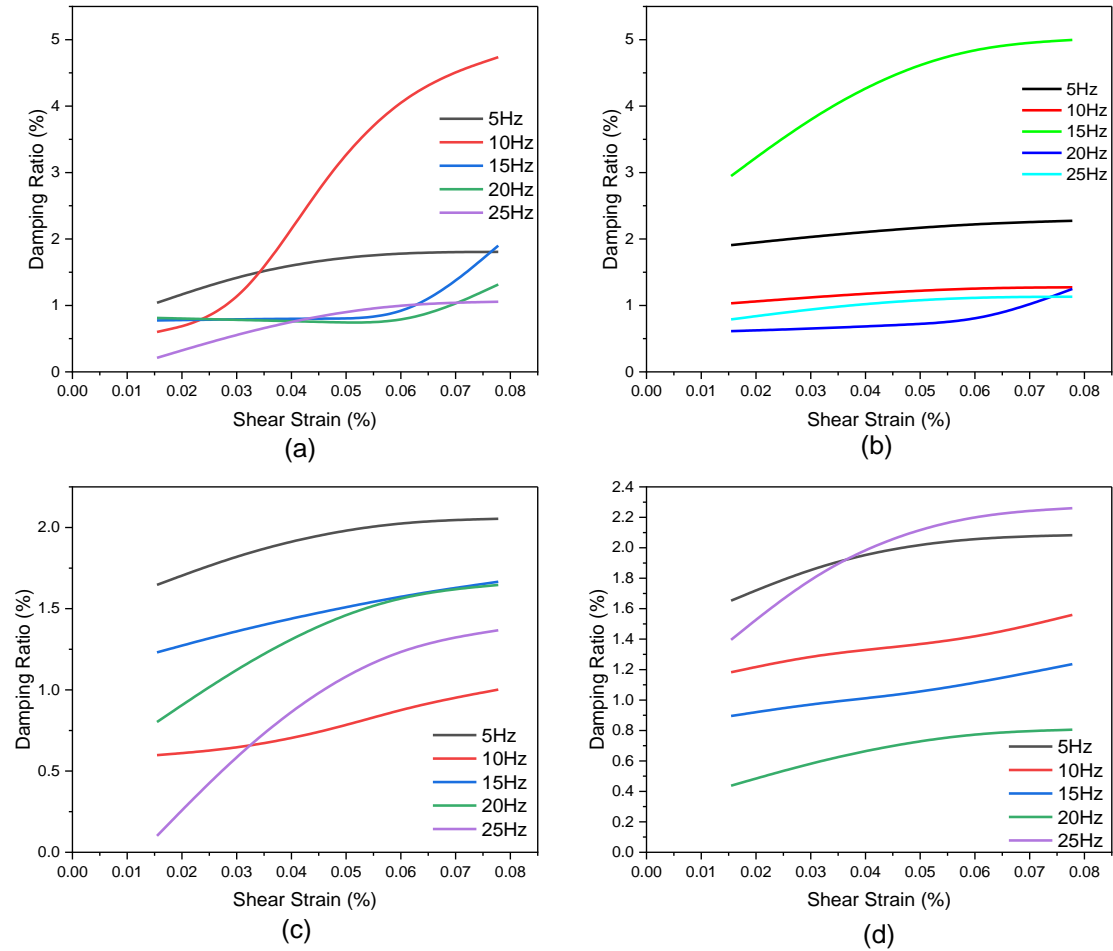
Fig. 31. Damping ratio-shear strain variation at various frequencies between 5 and 25 Hz when (a) $\gamma = 16$ kN/m^3, (b) $\gamma = 18$ kN/m^3, (c) $\gamma = 20$ kN/m^3, and (d) $\gamma = 22$ kN/m^3

The overall damping ratio vs. shear strain trend is close to the normalised damping ratio shear strain curve. As shear pressure increases, the damping ratio also rises. The damping ratio falls between 0.5 and 5 %. It may be said that the damping ratio declined as density grew. It is difficult to foresee a broad pattern when there is a change in frequency. It is resulting in a cumulative effect.

4.4 MACHINE LEARNING APPROACH

The obtained numerical findings, which demonstrate good agreement with experimental results, can be utilized for estimating displacement. The analysis of the data involves employing fine and medium decision tree (DT) topologies, as well as the Matérn 5/2 GPR,

rational quadratic GPR, squared exponential GPR, exponential GPR, and boosted tree models. Once the regression model is trained, a response plot is generated to visualize the predicted response relative to the recorded values. To make each prediction, a model trained without using the corresponding observation is used, typically through the application of holdout or cross-validation techniques.

In this particular study, a two-fold cross-validation approach is employed. A feedforward backpropagation network is trained using a backpropagation training algorithm. The input variables considered in the analysis consist of tank width ranging from 0 to 0.6 meters, frequency ranging from 5 to 25 Hz, a fixed D_{50} value of 0.285, unit weight of 18 kN/m3, optimum moisture content (OMC) of the geomaterial at 10.4%, and amateur pressure of 30 kPa. The target data for the regression model is the displacement of the geomaterial.

The predicted vs. true response plot is a valuable tool for assessing the performance of a regression model after training. This graph allows us to visualize how well the model predicts different response values. In an ideal scenario, all data points would fall precisely along a diagonal line, indicating that the predicted response matches the actual response.

Fig. 32 displays the predicted vs. true response plots for the fine and medium decision tree architectures, Matérn 5/2 GPR, rational quadratic GPR, squared exponential GPR, exponential GPR, and boosted tree models. By examining this plot, we can evaluate the performance of each model and compare their ability to accurately predict the response values. Ideally, we would observe a tight cluster of points along the diagonal line, indicating strong predictive accuracy.

The residuals plot is another method for assessing model performance after training. Residuals represent the discrepancy between the predicted and actual response values. In a successful model, the residuals would typically exhibit a symmetrical distribution around zero. This suggests that the model's predictions are unbiased and have a consistent level of accuracy.

Fig. 33 illustrates the residual vs. true response plot for the fine and medium decision tree architectures, Matérn 5/2 GPR, rational quadratic GPR, squared exponential GPR, exponential GPR, and boosted tree models. By analyzing this plot, we can assess the model's performance in terms of the magnitude and distribution of the residuals. A

symmetrical distribution of residuals around zero would indicate a well-performing model with minimal bias.

By examining both the predicted vs. true response plot and the residuals plot, we can gain insights into the accuracy and reliability of the regression models across different architectures and approaches.
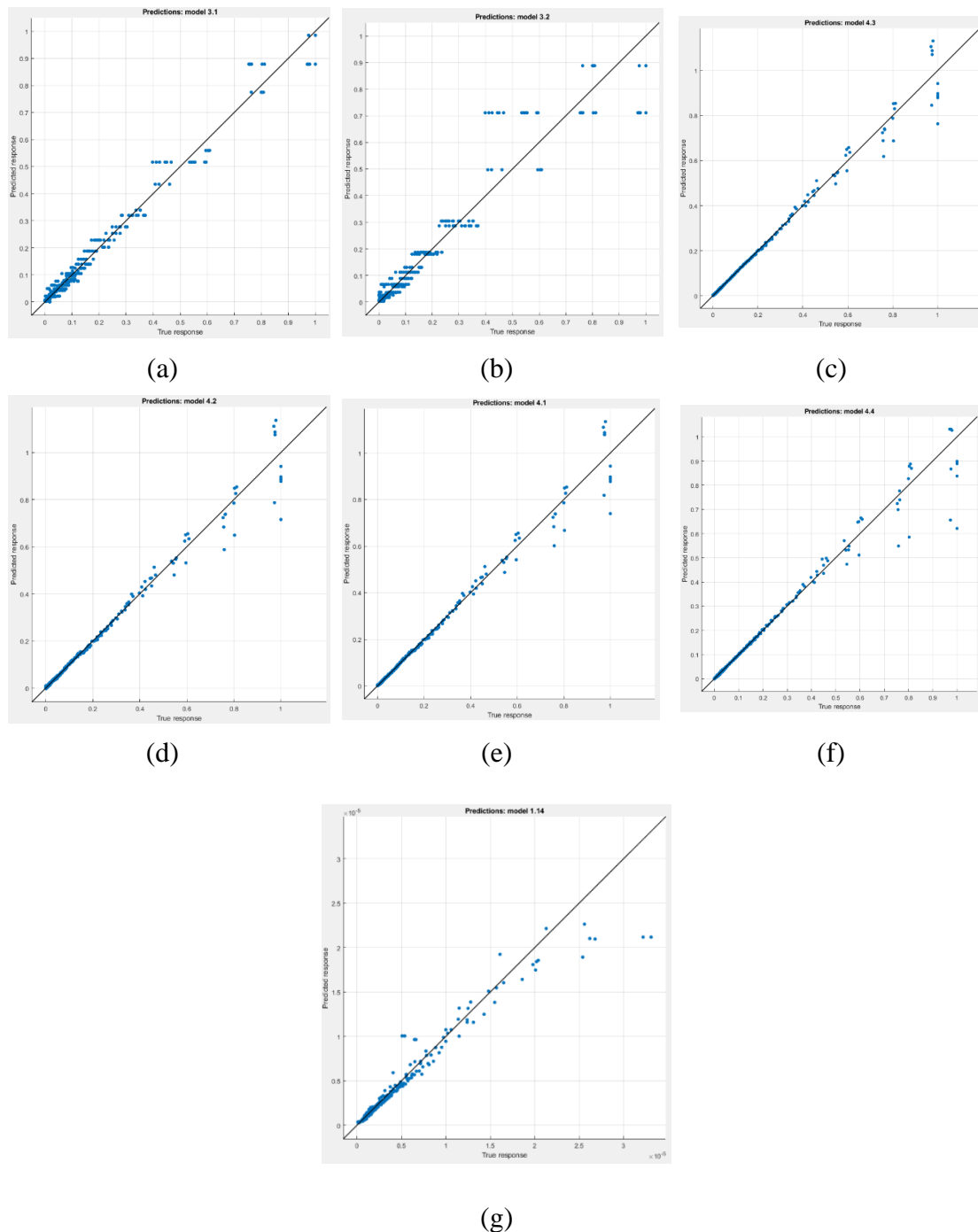
Fig. 32. Predicted vs true response plot of (a) fine tree, (b) medium tree, (c) matern 5/2 GPR, (d) squared exponential GPR (e) the rational quadratic GPR, (f) exponential GPR, and (g) boosted tree
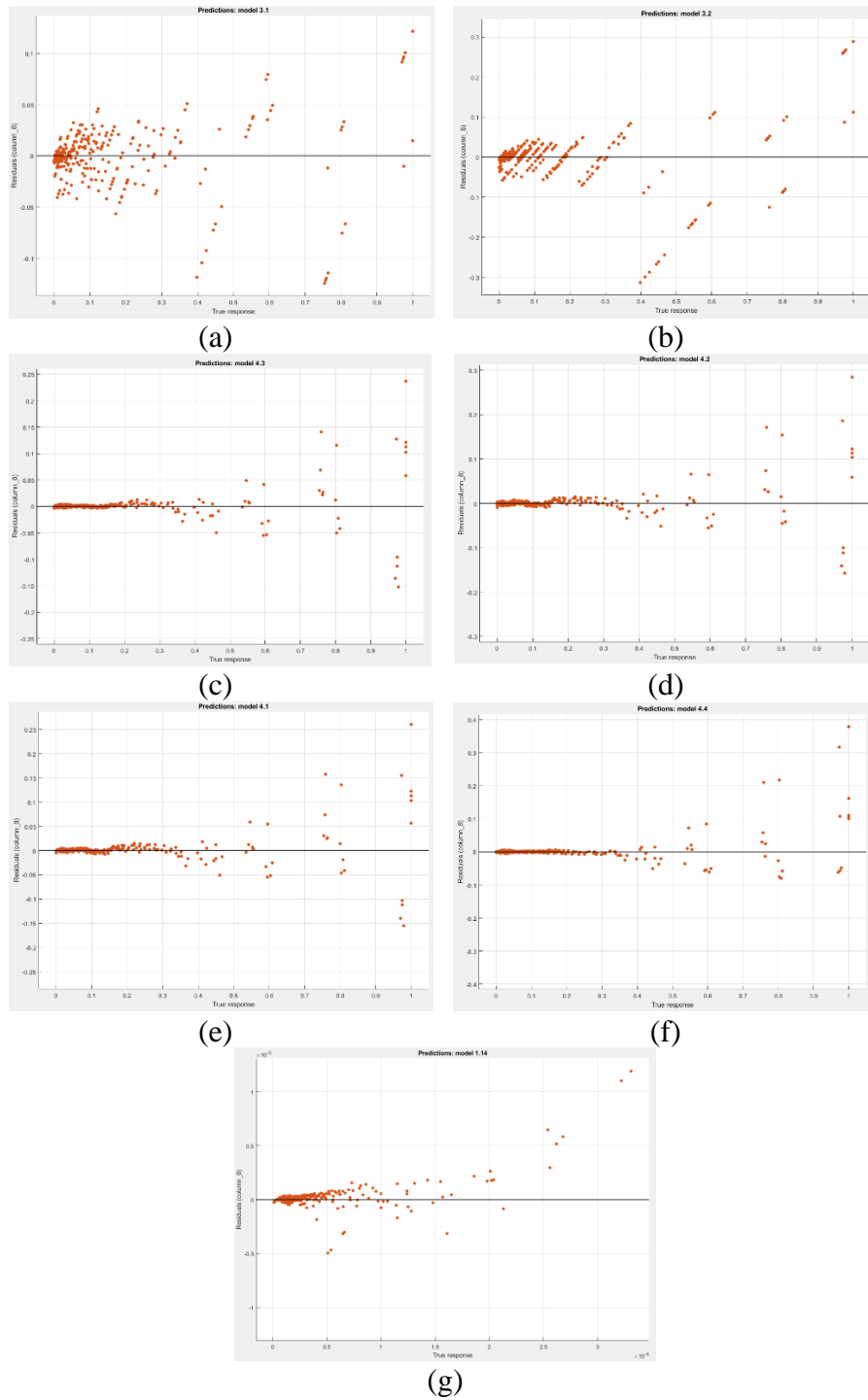
Fig. 33. Residual vs true response plot of (a) fine tree, (b) medium tree, (c) matern 5/2 GPR, (d) squared exponential GPR, (e) the rational quadratic GPR, (f) exponential GPR, and (g) boosted tree

Model parameters play a crucial role in evaluating the efficacy of a model. After training the network, it is important to assess the performance of each method based on specific metrics. In Table 8, the performance of each method is likely summarized, providing valuable insights into their effectiveness.

Table 8. Comparison of performance of models

Model	RSME	R^2	MSE	MAE	Train time (s)
Fine Tree	0.031891	0.98	0.0010171	0.019795	0.39606
Medium Tree	0.071315	0.91	0.0050858	0.036892	0.077911
Rational Quadratic GPR	0.030544	0.98	0.00093291	.010344	0.99513
Square Exponential GPR	0.032592	0.98	0.0010622	0.011338	0.24763
Matern 5/2 GPR	0.028357	0.99	0.00080412	0.0091226	0.23602
Exponential GPR	0.039679	0.97	0.0015745	0.011376	0.20824
Boosted Tree	1.32×10^{-6}	0.94	1.7424×10^{-12}	5.07×10^{-12}	0.92155

The RMSE (root mean squared error) is always positive because it represents the square root of the average of the squared differences between the actual and forecasted values in a regression model. As the name suggests, it measures the average size of the errors, and therefore, it cannot be negative.

Similarly, the R^2 (coefficient of determination) is a metric that quantifies the proportion of variance in the dependent variable that can be explained by the independent variables in a regression model. The R^2 value ranges from 0 to 1, where 0 indicates that the model explains none of the variance, and 1 indicates that the model explains all of the variance. The R^2 value cannot exceed 1 since it represents the maximum amount of variance that can be explained by the model.

The MAE (mean absolute error) is also a positive metric and is less sensitive to outliers compared to RMSE. It measures the average absolute difference between the actual and forecasted values, providing a more robust measure of prediction accuracy.

Fig. 34 presents a comparison of the numerical and machine learning model's displacement projections. Each model is tested across a range of frequencies from 5 to 25 Hz. This figure can be used to visually assess the performance and agreement between the numerical and machine learning models in predicting the displacements at different frequencies.
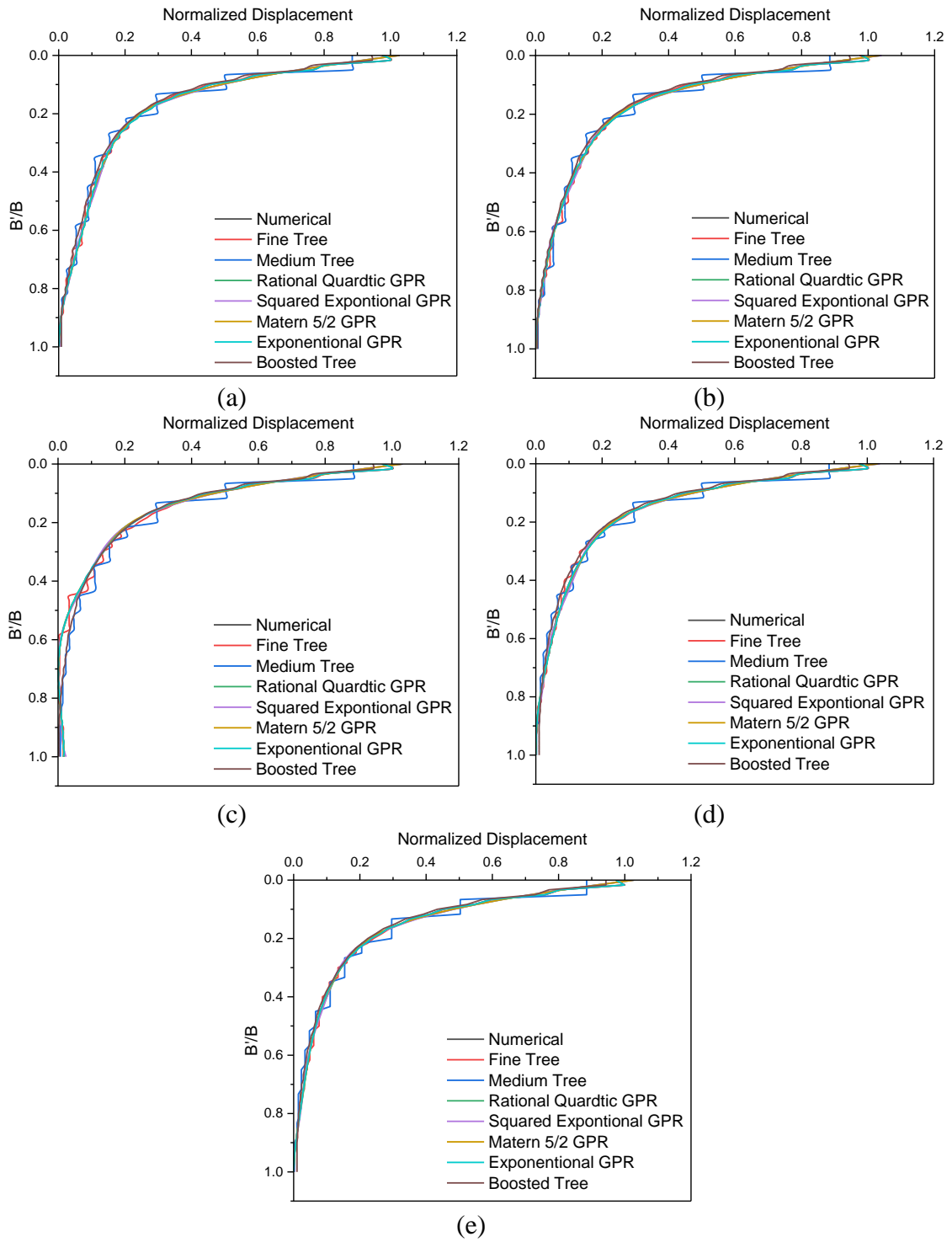
Fig. 34. Comparison of experimental and ML model results on displacement variation along depth ratio at (a) 5 Hz, (b) 10 Hz, (c) 15 Hz, (d) 20 Hz, and (e) 25 Hz

CHAPTER 5

CONCLUSIONS AND RECOMMENDATIONS FOR FUTURE WORK

5.1 CONCLUSIONS

This study was conducted on poorly graded (SP) clean sand obtained from the banks of Yamuna River. Geogrid was placed in the geomaterial to investigate the strength improvement as reinforcement for confined geomaterial. The unreinforced geomaterial in confined state is compared with geogrid reinforced to find the optimum number of layers and the location of placement. A numerical study along with experimental investigation has showed significance of displacement, stress-strain, and damping of confined geomaterial subjected to vibratory loads for varied engineering applications. Additionally, the study utilized a machine learning model and examined various forecasting models to assess their efficiency. Further, the following conclusions can be drawn as:

- The geogrid reinforced section shows better performance than the unreinforced section in terms of strength and stiffness.
- In the single-layer reinforcement, it is observed that the maximum strength is achieved when the geogrid is placed at a depth of 50 mm from the surface.
- In the double-layered reinforced sections, the combination of geogrid placed at 50 and 100 mm from the top gives the optimum results compared to the other combinations in location A. However, at locations B, C, D and E (corners), the reinforcement at depths 50 and 150 mm shows better resistance to penetration. The reinforcement effect started after the initial settlement of geogrids from 50 mm to 60 and 62 mm for locations A and B, respectively.
- From the results obtained for location A double layer reinforcement at 50 and 100 mm and for locations B, C, D and E triple layered reinforcement is the most efficient.

- The displacement-depth ratio showed that changes in displacement along the depth are not significant. The displacement-depth ratio increases up to 80 % for a frequency range of 5 - 25 Hz.

- The displacement-depth ratio of numerical findings showed a departure of 4 - 41.4 % from experimental findings for varied input frequencies.

- The damping ratio of the confined granular fill has been found in the range of 0.5 - 50 % for various input parameters considered in the study.

- The percentage change in damping ratio from 5 - 25 Hz has been found in the range of 1 - 50 %. Further, the increase in unit weight (16 – 22 kN/m3) showed a compounded variation in the percentage change of damping ratio (9 – 80 %).

- The matern 5/2 GPR model demonstrates the highest level of accuracy, as evidenced by its impressive R2 value of 0.99. This R2 value indicates a strong correlation between the predictions of the matern 5/2 GPR model and the actual outcomes, suggesting that it is the most reliable model for accurate predictions.

- In this analysis, the mean squared error (MSE) is utilized as a performance metric to evaluate the models. A smaller MSE value indicates a better-performing model. Among the models, the boosted tree model achieved the lowest MSE with a value of 1.7424×10-12. This exceedingly low value indicates that the boosted tree model exhibits the smallest overall prediction error.

- When considering the mean absolute error (MAE) as a measure of model performance, the boosted tree model also attains the lowest value of 5.07×10-12. This implies that the boosted tree model displays the smallest average absolute difference between its predictions and the actual values.

Thus, in unpaved roads where the surrounding material is the locally available soil, the double-layered reinforcements optimize the overall strength. However, kerbs in paved roads induce a boundary effect. The triple-layered reinforcement is efficient on such sites. Further, it can be generalized that the frequency of excitation, unit weight, young's modulus are key parameters while examining the dynamic behaviour of the confined geomaterial. The research conducted in the present study can be adopted by engineers and practitioners for estimating the dynamic properties of the confined geomaterial in construction practices.

5.2 RECOMMENDATIONS FOR FUTURE WORK

The relevance of displacement, stress-strain, and damping are examined in the findings of the numerical analysis coupled with experimental modelling of confined geomaterial subjected to vibratory stresses. Based on the results of the current study, it may be possible to suggest the following recommendations for further research.

- The investigation was conducted on poorly graded sand (SP). The properties of other types of geomaterial may be established by using a similar simulation approach which can be expanded upon for future research.
- For the study, the geogrids were inserted into the geomaterial up to a maximum depth of 150 mm; however, this depth may be extended, and future work may combine single, double, and triple layered geogrid reinforcement at various depths greater than 150 mm.
- The research may be expanded to examine the effects of additional variables besides frequency, elastic modulus, and density, which are considered in the present study.

REFERENCES

1. Ahmad, M. W., Reynolds, J., & Rezgui, Y. (2018). Predictive modelling for solar thermal energy systems: A comparison of support vector regression, random forest, extra trees and regression trees. Journal of cleaner production, 203, 810-821.

2. Ahmadi, M. M., & Dariani, A. G. (2017). Cone penetration test in sand: A numerical-analytical approach. Computers and Geotechnics, 90, 176-189.

3. Akbulut, S., Hasiloglu, A. S., & Pamukcu, S. (2004). Data generation for shear modulus and damping ratio in reinforced sands using adaptive neuro-fuzzy inference system. Soil Dynamics and Earthquake Engineering, 24(11), 805-814.

4. Alidoust, P., Keramati, M., Hamidian, P., Amlashi, A. T., Gharehveran, M. M., & Behnood, A. (2021). Prediction of the shear modulus of municipal solid waste (MSW): An application of machine learning techniques. Journal of Cleaner Production, 303, 127053.

5. Almeida, M. S. S., Jamiolkowski, M., & Peterson, R. W. (1991). Preliminary result of CPT tests in calcareous Quiou sand. In Proceedings of the First International Symposium on Calibration Chamber Testing/ISOCCTI, Potsdam, Germany. Elsevier Science Publishing Co, New York, 41-53.

6. Alshawmar, F., & Fall, M. (2022). Geotechnical behaviour of layered paste tailings in shaking table testing. International Journal of Mining, Reclamation and Environment, 36(3), 174-195.

7. Amir-Faryar, B., Aggour, M. S., & McCuen, R. H. (2017). Universal model forms for predicting the shear modulus and material damping of soils. Geomechanics and Geoengineering, 12(1), 60-71.

8. Assimaki, D., Kausel, E., & Whittle, A. (2000). Model for dynamic shear modulus and damping for granular soils. Journal of Geotechnical and Geoenvironmental Engineering, 126(10), 859-869.

9. Baghbani, A., Choudhury, T., Samui, P., & Costa, S. (2023). Prediction of secant shear modulus and damping ratio for an extremely dilative silica sand based on machine learning techniques. Soil Dynamics and Earthquake Engineering, 165, 107708.

10. Baldi, G., Bellotti, R., Ghionna, V., Jamiolkowski, M., & Pasqualine, E. (1982). Design parameters for sands from CPT. In Proceedings of the Second European Symposium on Penetration Testing. Balkema, Amsterdam, 425–432.

11. Bonita, J. A. (2000). The effects of vibration on the penetration resistance and pore water pressure in sands. Virginia Polytechnic Institute and State University.

12. Bourdeau, P. L., & Ashmawy, A. K. (2002). Unpaved roads. In Geosynthetics and their applications. Thomas Telford Publishing. 165-183.

13. Breiman, F. (1984). Olshen, and Stone. Classification and Regression trees.

14. Brennan, A. J., Thusyanthan, N. I., & Madabhushi, S. P. (2005). Evaluation of shear modulus and damping in dynamic centrifuge tests. Journal of Geotechnical and Geoenvironmental Engineering, 131(12), 1488-1497.

15. Collins, R., & Miller, G. A. (2020). Cone penetration testing in unsaturated soils at two Instrumented test sites. In Unsaturated Soils: Research & Applications. CRC Press. 1489-1494.

16. Conti, R., Viggiani, G. M., & Perugini, F. (2014). Numerical modelling of centrifuge dynamic tests of circular tunnels in dry sand. Acta Geotechnica, 9(4), 597–612.

17. Cuelho, E. V., & Perkins, S. W. (2017). Geosynthetic subgrade stabilization–Field testing and design method calibration. Transportation Geotechnics, 10, 22-34.

18. Darendeli, M. B. (2001). Development of a new family of normalized modulus reduction and material damping curves. The university of Texas at Austin.

19. Das, B. M., & Luo, Z. (2016). Principles of soil dynamics. Cengage Learning.

20. Dietterich, T. G. (2000). Ensemble methods in machine learning. In Multiple Classifier Systems: First International Workshop, MCS 2000 Cagliari, Italy, June 21–23, 2000 Proceedings 1 (pp. 1-15). Springer Berlin Heidelberg.

21. Dong, X., Yu, Z., Cao, W., Shi, Y., & Ma, Q. (2020). A survey on ensemble learning. Frontiers of Computer Science, 14, 241-258.

22. Farfani, H. A., Behnamfar, F., & Fathollahi, A. (2015). Dynamic analysis of soil-structure interaction using the neural networks and the support vector machines. Expert Systems with Applications, 42(22), 8971-8981.

23. Fathi, H., Jamshidi Chenari, R., & Vafaeian, M. (2019). Shaking Table Study on PET Strips-Sand Mixtures Using Laminar Box Modelling. Geotechnical and Geological Engineering, 38(1), 683–694.

24. Giretti, D., Been, K., Fioravante, V., & Dickenson, S. (2018). CPT calibration and analysis for a carbonate sand. Géotechnique, 68(4), 345-357.

25. Gomes, R. C., Santos, J. A., Modaressi-Farahmand Razavi, A., & Lopez-Caballero, F. (2015). Validation of a strategy to predict secant shear modulus and damping of soils with an elastoplastic model. KSCE Journal of Civil Engineering, 20(2), 609–622.

26. Gupta, R., & Trivedi, A. (2011). Effect of non-plastic fines on the behavior of loose sand—an experimental study. Electron J Geotech Eng 14, 1–15.

27. Hardin, B. O., & Black, W. L. (1968). Vibration modulus of normally consolidated clay. Journal of the Soil Mechanics and Foundations Division, 94(2), 353-369.

28. Hardin, B. O., & Drnevich, V. P. (1972). Shear modulus and damping in soils: measurement and parameter effects (terzaghi leture). Journal of the soil mechanics and foundations division, 98(6), 603-624.

29. Hasthi, V., Raja, M. N. A., Hegde, A., & Shukla, S. K. (2022). Experimental and intelligent modelling for predicting the amplitude of footing resting on geocell-reinforced soil bed under vibratory load. Transportation Geotechnics, 35, 100783.

30. Ibrahim, A. F., Abdelaal, A., & Elkatatny, S. (2022). Formation resistivity prediction using decision tree and random forest. Arabian Journal for Science and Engineering, 47(9), 12183-12191.

31. IS 2720, Part – 4 (1985). Methods of test for soils: grain size analysis. New Delhi: Bureau of Indian Standards.

32. IS 2720, Part – 7 (1980). Methods of test for soils: determination of water content-dry density relation using light compaction. New Delhi: Bureau of Indian Standards.

33. IS 4968, Part – 3 (1976) Method for Subsurface Sounding for Soils Part 3 Static Cone Penetration Test. New Delhi: Bureau of Indian Standards (Reaffirmed 1987).

34. IS: 2720, Part – 13 (1986). Methods of tests for soils: direct shear test. New Delhi: Bureau of Indian Standards.

35. Ishibashi, I., & Zhang, X. (1993). Unified Dynamic Shear Moduli and Damping Ratios of Sand and Clay. Soils and Foundations, 33(1), 182–191.

36. Iwasaki, T., Tatsuoka, F., & Takagi, Y. (1978). Shear moduli of sands under cyclic torsional shear loading. Soils and Foundations, 18(1), 39-56.

37. Kluger, M. O., Kreiter, S., Stähler, F. T., Goodarzi, M., Stanski, T., & Mörz, T. (2021). Cone penetration tests in dry and saturated Ticino sand. Bulletin of Engineering Geology and the Environment, 80(5), 4079–4088.

38. Koga, Y., & Matsuo, O. (1990). Shaking table tests of embankments resting on liquefiable sandy ground. Soils and Foundations, 30(4), 162-174.

39. Kumar, A., Kumar, A., Jha, A. K., & Trivedi, A. (2020). Crack Detection of Structures using Deep Learning Framework. 2020 3rd International Conference on Intelligent Sustainable Systems (ICISS), 526-533.

40. Kumar, Y., Trivedi, A., Shukla, S.K.: Damage Evaluation in Pavement-Geomaterial System Using Finite Element-Scaled Accelerated Pavement Testing. Transp. Infrastruct. Geotech. (2023). https://doi.org/10.1007/s40515-023-00309-y

41. Kumari, N., & Trivedi, A. (2022). The Effect of Confined Granular Soil on Embedded PZT Patches Using FFT and Digital Static Cone Penetrometer (DSCP). Applied Sciences, 12(19), 9711.

42. Mase, L. Z. (2017). Shaking table test of soil liquefaction in Southern Yogyakarta. International Journal of Technology, 8(4), 747-760.

43. Miller, G. A., Tan, N. K., Collins, R. W., & Muraleetharan, K. K. (2018). Cone penetration testing in unsaturated soils. Transportation Geotechnics, 17, 85-99.

44. Molina-Gómez, F., da Fonseca, A. V., Ferreira, C., & Camacho-Tauta, J. (2020). Dynamic properties of two historically liquefiable sands in the Lisbon area. Soil Dynamics and Earthquake Engineering, 132, 106101.

45. Myles, A. J., Feudale, R. N., Liu, Y., Woody, N. A., & Brown, S. D. (2004). An introduction to decision tree modeling. Journal of Chemometrics: A Journal of the Chemometrics Society, 18(6), 275-285.

46. Ojha, S., & Trivedi, A. (2013). Shear strength parameters for silty-sand using relative compaction. Electronic Journal of Geotechnical Engineering, 18(1), 81-99.

47. Okur, D. V., & Ansal, A. (2007). Stiffness degradation of natural fine grained soils during cyclic loading. Soil Dynamics and Earthquake Engineering, 27(9), 843-854.

48. Oztoprak, S., & Bolton, M. D. (2013). Stiffness of sands through a laboratory test database. Géotechnique, 63(1), 54-70.

49. Pournaghiazar, M., Russell, A. R., & Khalili, N. (2013). The cone penetration test in unsaturated sands. Geotechnique, 63(14), 1209-1220.

50. Price, A. B., DeJong, J. T., & Boulanger, R. W. (2017). Cyclic loading response of silt with multiple loading events. Journal of geotechnical and geoenvironmental engineering, 143(10), 04017080.

51. Quinlan, J. R. (1993). C4. 5 Programs for Machine Learning. Morgan Kaufmann, San Mateo, California.

52. Quinonero-Candela, J., & Rasmussen, C. E. (2005). A unifying view of sparse approximate Gaussian process regression. The Journal of Machine Learning Research, 6, 1939-1959.

53. Reddy, S. B., & Krishna, A. M. (2021). Sand–scrap tyre chip mixtures for improving the dynamic behaviour of retaining walls. International Journal of Geotechnical Engineering, 15(9), 1093-1105.

54. Rodriguez-Galiano, V., Sanchez-Castillo, M., Chica-Olmo, M., & Chica-Rivas, M. J. O. G. R. (2015). Machine learning predictive models for mineral prospectivity: An evaluation of neural networks, random forest, regression trees and support vector machines. Ore Geology Reviews, 71, 804-818.

55. Rollins, K. M., Evans, M. D., Diehl, N. B., & III, W. D. D. (1998). Shear modulus and damping relationships for gravels. Journal of geotechnical and Geoenvironmental Engineering, 124(5), 396-405.

56. Safavian, S. R., & Landgrebe, D. (1991). A survey of decision tree classifier methodology. IEEE transactions on systems, man, and cybernetics, 21(3), 660-674.

57. Sagi, O., & Rokach, L. (2018). Ensemble learning: A survey. Wiley Interdisciplinary Reviews: Data Mining and Knowledge Discovery, 8(4), e1249.

58. Seed, H. B., Wong, R. T., Idriss, I. M., & Tokimatsu, K. (1986). Moduli and damping factors for dynamic analyses of cohesionless soils. Journal of geotechnical engineering, 112(11), 1016-1032.

59. Shaqour, F. M. (2007). Cone penetration resistance of calcareous sand. Bulletin of Engineering Geology and the Environment, 66(1), 59-70.

60. Sharma, S., Venkateswarlu, H., & Hegde, A. (2019). Application of machine learning techniques for predicting the dynamic response of geogrid reinforced foundation beds. Geotechnical and Geological Engineering, 37, 4845-4864.

61. Sigurdsson, O. (1993). Geosynthetic stabilization of unpaved roads on soft ground: A field evaluation (Doctoral dissertation, University of British Columbia).

62. Singh, M., Trivedi, A., & Shukla, S. K. (2020). Influence of geosynthetic reinforcement on unpaved roads based on CBR, and static and dynamic cone penetration tests. International Journal of Geosynthetics and Ground Engineering, 6(2), 13.

63. Singh, M., Trivedi, A., & Shukla, S. K. (2022). Evaluation of geosynthetic reinforcement in unpaved road using moving wheel load test. Geotextiles and Geomembranes, 50(4), 581-589.

64. Singh, M., Trivedi, A., Shukla, S.K.: Effect of geosynthetic reinforcement on strength behaviour of sub- grade-aggregate composite system. In: Sustainable Civil Engineering Practices. pp. 61-70 (2020a). https://doi.org/10.1007/978-981-15-3677-9_7

65. Singh, M., Trivedi, A., Shukla, S.K.: Evaluation of geosynthetic reinforcement in unpaved road using moving wheel load test. Geotext. Geomembr. (2022). https://doi.org/10.1016/j.geotexmem.2022.02.005

66. Singh, M., Trivedi, A., Shukla, S.K.: Fuzzy-based model for predicting strength of geogrid-reinforced subgrade soil with optimal depth of geogrid reinforcement. Transp. Infrastruct. Geotechnol. 7(4), 664–683 (2020c). https://doi.org/10.1007/s40515-020-00113-y

67. Singh, M., Trivedi, A., Shukla, S.K.: Influence of geosynthetic reinforcement on unpaved roads based on CBR, and static and dynamic cone penetration tests. Int J. Geosynth. Ground Eng. 6(2), 1–13 (2020b). https://doi.org/10.1007/s40891-020-00196-0

68. Swain, P. H., & Hauska, H. (1977). The decision tree classifier: Design and potential. IEEE Transactions on Geoscience Electronics, 15(3), 142-147.

69. Trivedi, A., & Singh, S. (2004). Cone resistance of compacted ash fill. Journal of Testing and Evaluation, 32(6), 429-437.

70. Vucetic, M., & Dobry, R. (1991). Effect of soil plasticity on cyclic response. Journal of geotechnical engineering, 117(1), 89-107.

71. Vucetic, M., & Mortezaie, A. (2015). Cyclic secant shear modulus versus pore water pressure in sands at small cyclic strains. Soil Dynamics and Earthquake Engineering, 70, 60-72.

72. Wichtmann, T., & Triantafyllidis, T. (2004). Influence of a cyclic and dynamic loading history on dynamic properties of dry sand, part I: cyclic and dynamic torsional prestraining. Soil Dynamics and Earthquake Engineering, 24(2), 127-147.

73. Wichtmann, T., & Triantafyllidis, T. (2004). Influence of a cyclic and dynamic loading history on dynamic properties of dry sand, part II: cyclic axial preloading. Soil Dynamics and Earthquake Engineering, 24(11), 789-803.

74. Wichtmann, T., & Triantafyllidis, T. (2013). Effect of uniformity coefficient on G/G max and damping ratio of uniform to well-graded quartz sands. Journal of geotechnical and geoenvironmental engineering, 139(1), 59-72.

75. Wilson, A. G., Knowles, D. A., & Ghahramani, Z. (2011). Gaussian process regression networks. arXiv preprint arXiv:1110.4411.

76. Xu, Min, Pakorn Watanachaturaporn, Pramod K. Varshney, and Manoj K. Arora. "Decision tree regression for soft classification of remote sensing data." Remote Sensing of Environment 97, no. 3 (2005): 322-336.

77. Yang, E.-K., Choi, J.-I., Kwon, S.-Y., & Kim, M.-M. (2011). Development of dynamic p-y backbone curves for a single pile in dense sand by 1g shaking table tests. KSCE Journal of Civil Engineering, 15(5), 813–821.

78. Yoo, M. T., Choi, J. I., Han, J. T., & Kim, M. M. (2013). Dynamic py curves for dry sand from centrifuge tests. Journal of earthquake engineering, 17(7), 1082-1102.

79. Younas, N., Ali, A., Hina, H., Hamraz, M., Khan, Z., & Aldahmani, S. (2022). Optimal causal decision trees ensemble for improved prediction and causal inference. IEEE Access, 10, 13000-13011.

80. Zeghal, M., & Elgamal, A. W. (1994). Analysis of site liquefaction using earthquake records. Journal of geotechnical engineering, 120(6), 996-1017.

81. Zeghal, M., Elgamal, A. W., Tang, H. T., & Stepp, J. C. (1995). Lotung downhole array. II: Evaluation of soil nonlinear properties. Journal of geotechnical engineering, 121(4), 363-378.

82. Zhang, J., Andrus, R. D., & Juang, C. H. (2005). Normalized shear modulus and material damping ratio relationships. Journal of geotechnical and geoenvironmental engineering, 131(4), 453-464.

LIST OF PUBLICATIONS

1. Boban, A., Kumar, Y., and Trivedi, A. (2023). "Numerical and Experimental Investigation of Confined Geomaterial Subjected to Vibratory Loading". Sustainable Infrastructure: Innovation, Opportunities, and Challenges (SIIOC-2023).

2. Boban, A., Gaur, K., and Trivedi, A. (2023). "Placement Depth and Layering Effect of Geogrid Reinforcement in Soft Subgrade Using Digital Static Cone Penetration Lab Test". Sustainable Infrastructure: Innovation, Opportunities, and Challenges (SIIOC-2023).

International Conference on
SUSTAINABLE INFRASTRUCTURE: INNOVATIONS,
OPPORTUNITIES AND CHALLENGES (SIIOC 2023)

CERTIFICATE
OF PARTICIPATION
Presented to

Ms *Ammu Boban*

For successfully participating and presenting a paper entitled, "NUMERICAL AND EXPERIMENTAL INVESTIGATION OF A CONFINED GEOMATERIAL SUBJECTED TO VIBRATORY LOAD", authored by Ammu Boban, Yakshansh Kumar, Prof. Ashutosh Trivedi at the International Conference on Sustainable Infrastructure: Innovations, Opportunities, and Challenges (SIIOC 2023) held during 20 - 21 April 2023 at NITK, Surathkal.

Dr. Raviraj H. M   **Dr. Pavan G. S**
Organizing Secretaries

Prof. B. R. Jayalekshmi
HOD, Civil Engg. Dept.

International Conference on
SUSTAINABLE INFRASTRUCTURE: INNOVATIONS,
OPPORTUNITIES AND CHALLENGES (SIIOC 2023)

CERTIFICATE
OF PARTICIPATION
Presented to

Ms *Ammu Boban*

For successfully participating and presenting a paper entitled, "PLACEMENT DEPTH AND LAYERING EFFECT OF GEOGRID REINFORCEMENT IN SOFT SUBGRADE USING DIGITAL STATIC CONE LAB PENETRATION TEST", authored by Ammu Boban,Kshitij Gaur,Prof. Ashutosh Trivedi at the International Conference on Sustainable Infrastructure: Innovations, Opportunities, and Challenges (SIIOC 2023) held during 20 - 21 April 2023 at NITK, Surathkal.

Dr. Raviraj H. M   **Dr. Pavan G. S**
Organizing Secretaries

Prof. B. R. Jayalekshmi
HOD, Civil Engg. Dept.

PAPER NAME

Dynamic Analysis of Confined Geomateri
al Subjected to Vibratory Loading i (1).pd
f

AUTHOR

Ammu Boban

WORD COUNT

7627 Words

CHARACTER COUNT

39282 Characters

PAGE COUNT

40 Pages

FILE SIZE

2.4MB

SUBMISSION DATE

May 29, 2023 2:37 PM GMT+5:30

REPORT DATE

May 29, 2023 2:38 PM GMT+5:30

● 15% Overall Similarity

The combined total of all matches, including overlapping sources, for each database.

- 5% Internet database
- Crossref database
- 8% Submitted Works database

- 10% Publications database
- Crossref Posted Content database